ARTICLE

Cyclin D3 drives inertial cell cycling in dark zone germinal center B cells

Juhee Pae[1], Jonatan Ersching[1], Tiago B.R. Castro[1], Marta Schips[2], Luka Mesin[1], Samuel J. Allon[3,4,5], Jose Ordovas-Montanes[5,6,7,8], Coraline Mlynarczyk[9], Ari Melnick[9], Alejo Efeyan[10], Alex K. Shalek[3,4,5,7,8], Michael Meyer-Hermann[2,11,12], and Gabriel D. Victora[1]

During affinity maturation, germinal center (GC) B cells alternate between proliferation and somatic hypermutation in the dark zone (DZ) and affinity-dependent selection in the light zone (LZ). This anatomical segregation imposes that the vigorous proliferation that allows clonal expansion of positively selected GC B cells takes place ostensibly in the absence of the signals that triggered selection in the LZ, as if by "inertia." We find that such inertial cycles specifically require the cell cycle regulator cyclin D3. Cyclin D3 dose-dependently controls the extent to which B cells proliferate in the DZ and is essential for effective clonal expansion of GC B cells in response to strong T follicular helper (Tfh) cell help. Introduction into the *Ccnd3* gene of a Burkitt lymphoma–associated gain-of-function mutation (T283A) leads to larger GCs with increased DZ proliferation and, in older mice, clonal B cell lymphoproliferation, suggesting that the DZ inertial cell cycle program can be coopted by B cells undergoing malignant transformation.

Introduction

Germinal centers (GCs) are the sites of affinity maturation, the process by which antibodies improve their affinity for antigen over time (Cyster and Allen, 2019; De Silva and Klein, 2015; Eisen, 2014; Mesin et al., 2016; Rajewsky, 1996; Shlomchik et al., 2019; Victora and Nussenzweig, 2012). For efficient affinity maturation, GC B cells must cycle between two major transcriptional states, associated with localization of B cells to each of the two microanatomical "zones" of the GC. When in the dark zone (DZ), B cells proliferate vigorously and mutate their immunoglobulin genes by somatic hypermutation (SHM). After transition to the light zone (LZ), B cells bearing advantageous mutations are selectively driven to clonally expand, based at least in part on their ability to bind and present antigen to GC-resident T follicular helper (Tfh) cells (Victora et al., 2010). Successive cycles of SHM and affinity-based selection ultimately enrich for higher-affinity cells among the GC B cell population in a process known as cyclic reentry (MacLennan, 1994; Victora and Nussenzweig, 2012).

A unique consequence of the anatomical compartmentalization of the GC is that mitogenic signals are segregated from the proliferation they induce. Upon positive selection, B cells typically transition from G1 to S phase of the cell cycle in the LZ, migrate from LZ to DZ while in S phase, and undergo G2 and M phases in the DZ (Gitlin et al., 2014; Victora et al., 2010). After this first division, cell cycling continues in the DZ, with most B cells undergoing on average two additional cell cycles before returning to the LZ for further selection (Gitlin et al., 2014). GC B cells that receive stronger signals from Tfh cells in the LZ, however, can undergo a much greater number of proliferative cycles in the DZ, resulting in exponential clonal expansion (Gitlin et al., 2014; Meyer-Hermann et al., 2012; Victora et al., 2010). At its extreme, this regulated expansion can lead to "clonal bursts," in which a single B cell can take over a 2,000-cell GC in the course of a few days (Tas et al., 2016). These bursts are associated with massive diversification of generally higher-affinity SHM variants and as such are likely to play an important role in the generation of high-affinity B cell clones (Amitai et al., 2017; Bannard and Cyster, 2017; Mesin et al., 2016).

Despite the importance of DZ proliferation for GC B cell selection and affinity maturation, our understanding of GC B cell

[1]Laboratory of Lymphocyte Dynamics, The Rockefeller University, New York, NY; [2]Department of Systems Immunology and Braunschweig Integrated Centre of Systems Biology, Helmholtz Centre for Infection Research, Braunschweig, Germany; [3]Institute for Medical Engineering and Science, Department of Chemistry, Koch Institute for Integrative Cancer Research, Massachusetts Institute of Technology, Cambridge, MA; [4]Ragon Institute of Massachusetts General Hospital, Massachusetts Institute of Technology and Harvard, Cambridge, MA; [5]Broad Institute of Massachusetts Institute of Technology and Harvard, Cambridge, MA; [6]Division of Gastroenterology, Boston Children's Hospital, Boston, MA; [7]Program in Immunology Harvard Medical School, Boston, MA; [8]Harvard Stem Cell Institute, Cambridge, MA; [9]Department of Medicine, Division of Hematology and Medical Oncology, Weill Cornell Medicine, New York, NY; [10]Spanish National Cancer Research Center, Madrid, Spain; [11]Institute for Biochemistry, Biotechnology and Bioinformatics, Technische Universität Braunschweig, Braunschweig, Germany; [12]Cluster of Excellence RESIST (EXC 2155), Hannover Medical School, Hannover, Germany.

Dr. Ersching died in October 2020; Correspondence to Gabriel D. Victora: victora@rockefeller.edu.

selection has historically focused on events that take place in the LZ (Mesin et al., 2016; Shlomchik et al., 2019). Consequently, the precise mechanisms that allow DZ proliferation to take place in the apparent absence of direct mitogenic signals are still incompletely understood. For instance, upon interaction with Tfh cells, positively selected LZ B cells express the transcription factor c-Myc (Calado et al., 2012; Dominguez-Sola et al., 2012; Finkin et al., 2019), as well as the mechanistic target of rapamycin (mTOR)–mediated anabolic program (Ersching et al., 2017). While both c-Myc and mTOR are required for LZ B cells to migrate to the DZ and enter the proliferative phase, the induction of these pathways appear to be mostly restricted to the LZ (Dominguez-Sola et al., 2012; Ersching et al., 2017; Finkin et al., 2019). This suggests that DZ B cells retain a memory of the intensity of the c-Myc and mTOR complex 1 (mTORC1)–dependent "charge" they received previously in the LZ and that they subsequently translate this memory into the number of cell cycles they will undergo in the DZ using a cell-intrinsic "timer" or "counter" (Bannard et al., 2013; Gitlin et al., 2014). The molecular pathways that directly control the number of cycles a GC B cell undergoes in the DZ remain uncharacterized.

Here, we used a combination of unbiased whole-transcriptome single-cell mRNA sequencing (scRNA-seq) analysis and targeted genetic and pharmacological manipulation of cell cycle regulators to investigate the molecular nature of DZ cell cycles. We find that DZ B cells adopt a distinct E2F^{high}/c-Myc^{low} mode of cell cycling that allows rapid and continuous proliferation in the absence of external mitogenic signals. We show that the cell cycle regulator cyclin D3, previously shown to be required for GC formation and maintenance (Cato et al., 2011; Peled et al., 2010), is a specific, dose-dependent controller of this phenotype and DZ cell cycling and that loss of cyclin D3 cannot be overcome by LZ cycling induced by strongly increased Tfh cell help. Introduction into mice of a gain-of-function mutation in cyclin D3 derived from human Burkitt lymphoma (Schmitz et al., 2012, 2014) leads to exacerbated B cell proliferation specifically in the GC DZ and development of clonal post-GC B cell expansions, linking the inertial proliferative program to malignant transformation.

Results

### B cell proliferation in the DZ is Tfh cell independent

To better understand GC B cell cycling in the DZ, we first sought to formally determine whether S phase entry by DZ B cells requires acute signals from Tfh cells in addition to those delivered in the LZ. To this end, we used a synchronized selection model (Ersching et al., 2017; Victora et al., 2010) to allow kinetically precise blocking of Tfh cell help to GC B cells at set time points after induced positive selection (Fig. 1 A). In this model, we use adoptive transfer of 4-hydroxy-3-nitro-phenylacetyl (NP)–specific B1-8^{hi} B cells followed by immunization with NP conjugated to chicken OVA (NP-OVA) to create GCs in which the majority of B cells lack the surface receptor DEC-205 (encoded by the gene Ly75). Treatment of mice with ongoing GCs with an antibody to DEC-205 fused to OVA (DEC-OVA) leads to presentation of OVA peptides by Ly75$^{+/+}$ GC B cells only. This induces Ly75$^{+/+}$ cells to preferentially interact with Tfh cells, triggering their positive selection (Pasqual et al., 2015; Victora et al., 2010). In this process, GC B cells also become synchronized: 12 h after DEC-OVA, most Ly75$^{+/+}$ cells are located in the LZ, where they interact extensively with Tfh cells (Ersching et al., 2017; Shulman et al., 2014). By 36 h after DEC-OVA, most Ly75$^{+/+}$ cells have transitioned to the DZ, where they begin their proliferative burst (Victora et al., 2010). Fig. 1, A–C; and Fig. S1 provide an overview of key time points in this kinetics. Entry into S phase of the cell cycle, revealed by double-pulsing mice with 5-ethynyl-2-deoxyuridine (EdU) and BrdU nucleotides (Gitlin et al., 2014), was greatly increased in DZ B cells at 36 h after DEC-OVA, indicating that, at this time point, GC B cells progress through the G1-S checkpoint while in the DZ compartment (Fig. 1, B and C; and Fig. S1, E and F). DZ S phase entry persisted above the steady-state level until at least 60 h after DEC-OVA treatment, when Ly75$^{+/+}$ cells remained predominantly in the DZ and continued to expand (Fig. 1, B and C; and Fig. S1, B–D).

To determine whether T cell help is continually required for DZ proliferation, we acutely blocked Tfh cell–B cell interaction either at the time of the initial Tfh signal delivery in the LZ (6 h after DEC-OVA) or following the transition of positively selected B cells to the DZ but before the proliferative burst (30 h after DEC-OVA; Fig. 1 D). As expected from the role of Tfh cell–mediated signaling in this model (Victora et al., 2010), early blocking of T cell–B cell interactions in the LZ using antibodies to MHC class II or CD40 ligand (CD40L) effectively prevented clonal expansion of Ly75$^{+/+}$ cells by 48 h after DEC-OVA treatment (Fig. 1, E and F). By contrast, blocking either pathway after B cells transitioned to the DZ had little, if any, effect on the expansion of Ly75$^{+/+}$ cells over Ly75$^{-/-}$ cells (Fig. 1, E and F) or the ability of Ly75$^{+/+}$ DZ B cells to enter S phase, as evidenced by EdU/BrdU incorporation (Fig. 1, G and H). We conclude that sustained proliferation of B cells in the GC DZ upon positive selection does not require continuous help from Tfh cells. We therefore refer to DZ cell cycles as "inertial," since they proceed in a cell-intrinsic fashion according to the strength of the initial "push" from Tfh cells, in contrast to the "primary" cell cycles that B cells undergo immediately downstream of selective signals in the LZ.

Inertial cycling is sustained by prolonged E2F activation following a decay in c-Myc activity

To identify the transcriptional programs associated with inertial cycling, we performed scRNA-seq on GC B cells at different time points after forcing positive selection using DEC-OVA. We index-sorted single Ly75$^{+/+}$ B cells using antibodies to LZ/DZ markers, and sorted cells were sequenced using the Smart-Seq2 protocol (Trombetta et al., 2014). We assayed GC B cells first at 12 h after DEC-OVA, when Ly75$^{+/+}$ B cells are enriched in the LZ in the process of receiving cognate help from Tfh cells, and then at 30, 46, and 60 h after DEC-OVA, as DZ B cells transition from signal-dependent proliferation to predominantly inertial modes of cycling before returning to the LZ between 72 and 96 h after DEC-OVA (Fig. 1, A–D; and Fig. S1; Victora et al., 2010). For comparison, we also included a sample of Ly75$^{-/-}$ counter-selected LZ cells from the 12-h time point (Table S1).
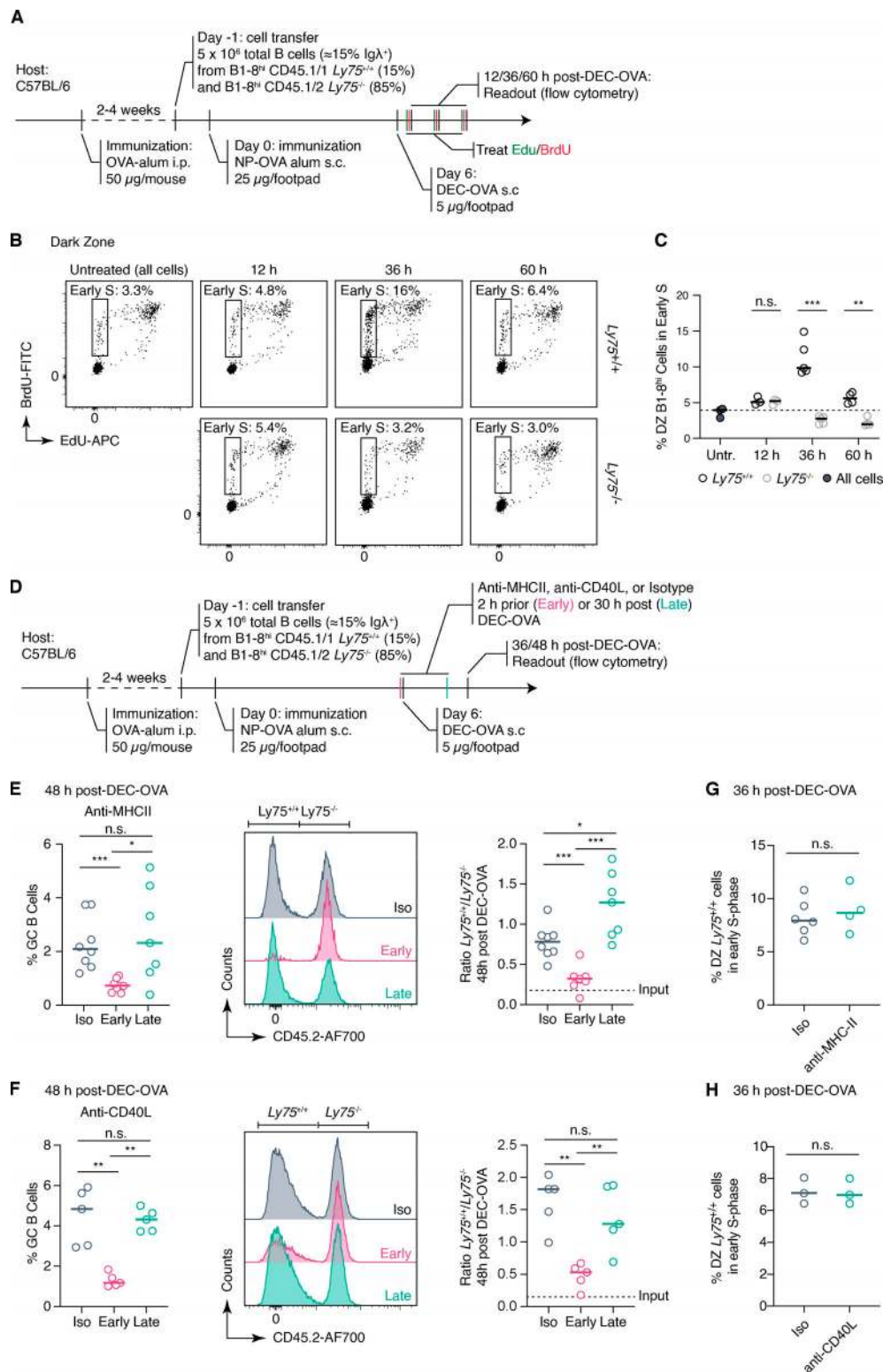
Figure 1. **Cell cycle entry by DZ B cells does not require Tfh cell help. (A)** Experimental setup for DEC-OVA–induced $Ly75^{+/+}$ GC B cells followed by double labeling with EdU/BrdU to assay for S phase entry. **(B)** S phase entry of $Ly75^{+/+}$ and $Ly75^{-/-}$ B1-8hi cells in the DZ, quantified in C. **(D)** Experimental setup for DEC-OVA–induced positive selection of $Ly75^{+/+}$ GC B cells followed by inhibition of T-B interaction using anti-MHC class II or anti-CD40L before (early) or after (late) DZ reentry. **(E and F)** Effect on GC size (left) and expansion of $Ly75^{+/+}$ cells over $Ly75^{-/-}$ cells (center, right) upon anti-MHC class II treatment (E) or anti-CD40L treatment (F). **(G and H)** S phase entry of $Ly75^{+/+}$ B1-8hi cells in the DZ upon late treatment with anti-MHC class II (G) or anti-CD40L (H). *, $P < 0.05$; **, $P < 0.01$; ***, $P < 0.001$; n.s., nonsignificant, a paired t test comparison between $Ly75^{+/+}$ and $Ly75^{-/-}$ cells in the same animal (C) or nonparametric Mann–Whitney test compared with the group treated with an isotype control (E–H). Bars indicate median. Each circle represents a mouse. Data are pooled from two (B and C), three (E and G), or two (F and H) independent experiments. Iso, isotope.
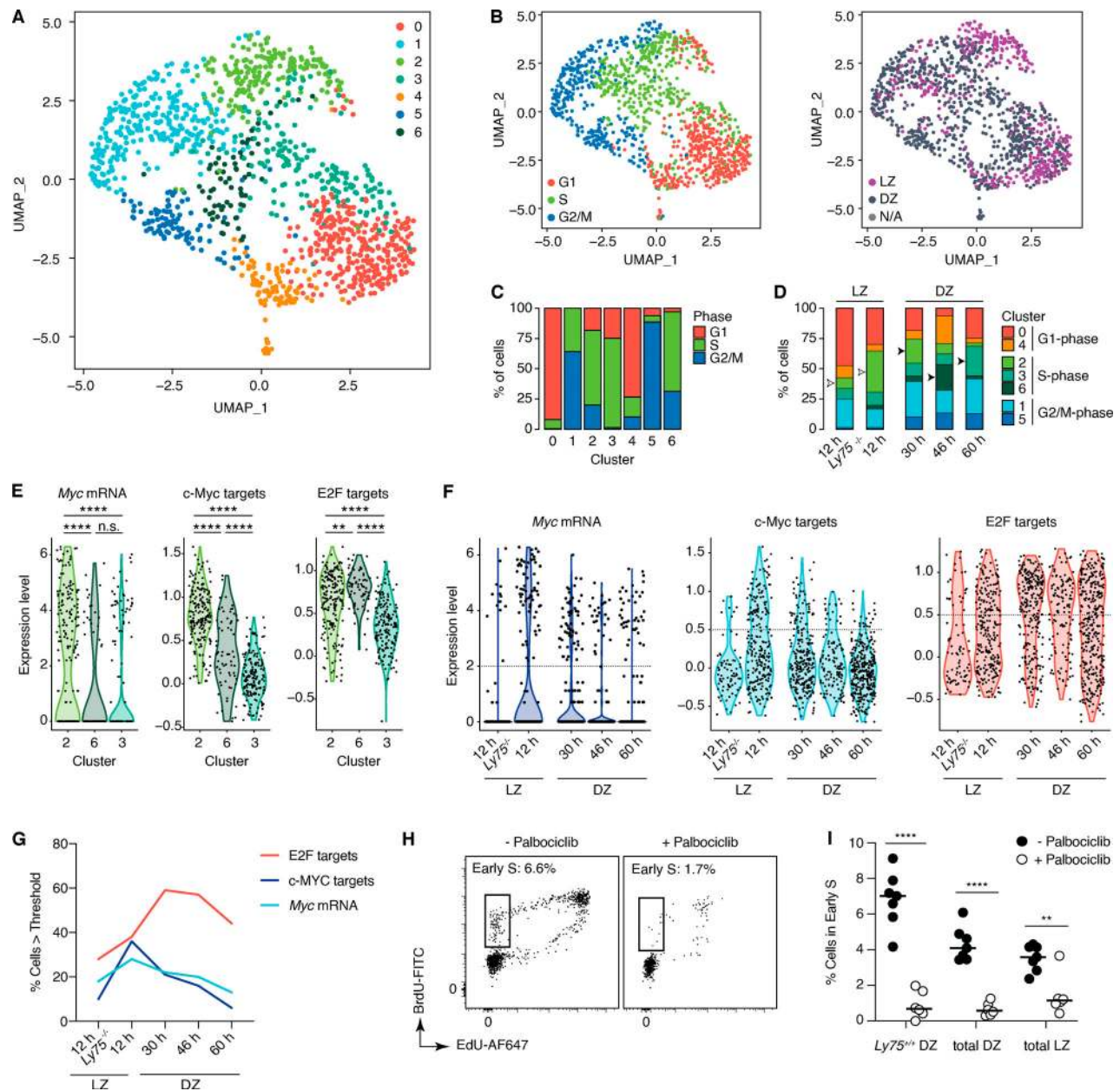
Figure 2. **Single-cell transcriptomic analysis of GC B cells undergoing positive selection. (A)** Uniform manifold approximation and projection (UMAP) plot displaying 1,220 cells colored by shared nearest neighbor clusters collected (default Wilcox test; see Materials and methods). Cells were collected from four independent experiments (see Table S1). **(B)** Distribution of cell cycle phase (left) and LZ/DZ phenotypes (right). **(C)** Distribution of cell cycle phase in clusters. **(D)** Changes in distribution of clusters grouped by cell cycle phase over the DEC-OVA–induced selection time course. **(E and F)** Expression of *Myc* mRNA, c-Myc, and E2F target gene signatures in clusters 2, 3, and 6 (E) or DEC-OVA time points with indicated zonal phenotypes (F). Dotted line indicates the threshold used for quantification in G. See Fig. S2 C for a complete list of P values. **(H)** S phase entry of *Ly75*^+/+ B1-8^hi cells in the DZ 12 h after treatment with palbociclib, a CDK4/6 inhibitor, or vehicle (PBS). **(I)** Quantification includes all LZ and DZ B1-8^hi cells, in addition to positively selected *Ly75*^+/+ B1-8^hi cells in the DZ. **, P < 0.01; ****, P < 0.0001, nonparametric Mann–Whitney test, compared with the PBS-treated control group. Bars indicate median. Each circle represents a mouse (H and I) or a cell (all other figures). Data are pooled from two independent experiments (H and I).

The 1,220 cells that passed our quality control thresholds fell into seven major clusters (Fig. 2 A). These were determined in large part by cell cycle phase as inferred from their transcriptional profile (Tirosh et al., 2016), with a lesser contribution of their LZ/DZ phenotype as defined by surface staining (Fig. 2 B). Clusters 0 and 4 contained primarily G1 cells; clusters 2, 3, and 6 were enriched in S phase cells; and clusters 1 and 5 were enriched in cells in the G2 and M phases (Fig. 2 C). To follow the

evolution of positively selected B cells across these clusters as they transitioned from reactive to inertial cell cycles and then to quiescence, we compared *Ly75*^+/+ and *Ly75*^−/− cells in the LZ at 12 h after DEC-OVA to *Ly75*^+/+ cells in the DZ at the 30-, 46-, and 60-h time points. This revealed a marked increase in representation of cells in cluster 2, as *Ly75*^+/+ cells are positively selected in the LZ at 12 h (empty arrowheads in Fig. 2 D). Enrichment in cluster 2 continued as cells transitioned to the DZ

at 30 h, after which the dominant S phase phenotype shifted to cluster 6 at 46 h and then cluster 3 at 60 h after DEC-OVA (filled arrowheads in Fig. 2 D). Pairwise comparisons of the three S phase clusters by gene set enrichment analysis (GSEA) using the "hallmark" signatures from the MSigDB database (Mootha et al., 2003; Subramanian et al., 2005) revealed expression of E2F and c-Myc target genes as the most consistent differences between the three clusters (Fig. S2 A). Cluster 2, enriched in LZ-phenotype cells from the 12- and 30-h time points, showed high expression of *Myc* and of c-Myc– and mTORC1-dependent transcriptional signatures (Fig. 2 E and Fig. S2 B; Peng et al., 2002; Schuhmacher et al., 2001). Given the strong association between these signatures and positive selection (Calado et al., 2012; Dominguez-Sola et al., 2012; Ersching et al., 2017; Finkin et al., 2019; Luo et al., 2018; Victora et al., 2010), this pattern suggests that cluster 2 consists primarily of recently selected B cells undergoing primary S phase, either on their way to or soon after DZ reentry. Cells in clusters 3 and 6, on the other hand, showed reduced levels of *Myc* and c-Myc– and mTORC1-dependent gene signatures while maintaining expression of E2F target genes (Fig. 2 E and Fig. S2 B), as expected if they were entering the cell cycle by inertia while being physically segregated from mitogenic signals located in the LZ. Kinetic analysis of *Myc* and c-Myc and E2F target gene signatures confirmed that E2F target gene expression levels remained unaltered between 30 and 46 h after DEC-OVA, while mRNA expression and activity of Myc decreased (Fig. 2, F and G; and Fig. S2 C). E2F signatures began to subside only at the 60-h time point, as inertial cycling defined by DZ S phase entry (Fig. 1, B and C) is already subsiding. Thus, unlike their LZ counterparts, DZ B cells appear to engage in a distinct mode of cell cycling that does not require continued expression of the *Myc* gene or its protein function to maintain E2F activity. This suggests that regulators of E2F that are downstream of c-Myc and other selection-dependent signals may be required to sustain proliferation after positively selected GC B cells transition to the DZ.

A major regulator of E2F activity are the D-type cyclins, which in partnership with cyclin-dependent kinases (CDKs) 4 and 6, activate E2F by phosphorylation of its negative regulator RB (Musgrove et al., 2011). To test whether D-type cyclins could be responsible for allowing the progression of inertial cell cycles, we treated mice with the inhibitor of CDK4/6 palbociclib 36 h after inducing positive selection of GC B cells with DEC-OVA and analyzed cell cycle progression 12 h later. Unlike blockade of MHC class II or CD40L (Fig. 1, D–H), palbociclib treatment strongly inhibited S phase entry in all GC B cells, including those undergoing inertial cycling in the DZ (Fig. 2, H and I). Thus, inertial S phase entry, while not dependent on Tfh-mediated signals, still requires activity of CDK4/6.

Ccnd3, but not *Ccnd2*, is required for DZ inertial cycling

Since B cells express exclusively cyclins D2 and D3 (encoded by *Ccnd2* and *Ccnd3*, respectively) upon mitogenic stimulation (Reid and Snow, 1996; Solvason et al., 1996), we sought to determine the relative contribution of these two cyclins to the CDK4/6 dependency of inertial cycles. *Ccnd2* mRNA was detectable primarily in the subset of cells undergoing S phase in the LZ in the

c-Myc[high] cluster 2 (Fig. S3 A). In agreement with our previous reports, *Ccnd2* was higher in *Ly75*^{+/+} cells at 12 h after DEC-OVA as well as in the LZ in general (Dominguez-Sola et al., 2012; Victora et al., 2010; Fig. S3, B and C). To investigate the function of cyclin D2 in GC B cells, we generated *Ccnd2* knockout mice using CRISPR-Cas9–mediated genome editing in zygotes to introduce a 4-bp deletion/frameshift in exon 1 of the gene (Fig. S3 D). *Ccnd2*^{−/−} mice lacked peritoneal B-1a cells (Fig. S3, E and F), and females were unable to produce progeny (data not shown), as shown previously using an independently generated knockout strain (Sicinski et al., 1996; Solvason et al., 2000), confirming that ours is a null allele. We adoptively transferred a 1:1 mixture of *Ccnd2*^{+/+} and *Ccnd2*^{−/−} B1-8^{hi} cells into WT hosts, which we then immunized with NP-OVA to generate GCs (Fig. S3 G), and found that zonal distribution was preserved in *Ccnd2*^{−/−} B1-8^{hi} B cells (Fig. S3, H and I). However, rather than reducing the ability of GC B cells to cycle, loss of cyclin D2 led to a small but consistent increase in the proportion of B1-8^{hi} cells entering S phase in both the LZ and DZ (Fig. S3, J–L). Despite this increase, absence of cyclin D2 showed no clear effect on the competitiveness of GC B cells over time when compared with *Ccnd2*-sufficient B cells within the same GC (Fig. S3, M and N). These experiments suggest that although cyclin D2 can affect the ability of GC B cells to enter cell cycle, it is not required for inertial cycling in the DZ.

In contrast to the dynamic behavior of *Ccnd2*, our scRNA-seq dataset showed that *Ccnd3* mRNA amounts were stably high throughout the LZ/DZ cycle and over our time course of DEC-OVA–induced selection, with only slight increases at the 30-h time point and in the DZ in general (Fig. 3, A–C). Despite these modest changes in mRNA expression, cyclin D3 protein levels were substantially higher in the DZ (Fig. 3 D), in agreement with previous reports based on histology (Peled et al., 2010). Also consistent with prior reports (Cato et al., 2011; Peled et al., 2010), we found that loss of *Ccnd3* led to dramatically reduced GC B cell frequency (Fig. 3, E and F). This is unlikely to be due to a general defect in proliferation, given that *Ccnd3*^{−/−} B cells proliferate normally in vitro and at pre-GC stages in vivo (Cato et al., 2011; Peled et al., 2010). Closer examination of *Ccnd3*^{−/−} GCs showed that decreased GC size was primarily caused by a marked reduction in the proportion of B cells with a DZ phenotype (Fig. 3, G and H), suggesting a strong block in the ability of *Ccnd3*^{−/−} B cells to undergo inertial cycling. This phenotype was identical when GCs were generated by adoptive transfer of *Ccnd3*^{−/−} B1-8^{hi} cells into WT hosts (Fig. 3 I), resulting in a significantly decreased DZ/LZ ratio (Fig. 3, J and K) and an almost complete loss in S phase initiation in the DZ with only a minor decrease of fitness in the LZ (Fig. 3, J and L–N). The requirement for cyclin D3 is therefore GC B cell intrinsic and largely restricted to the DZ. *Ccnd3*^{−/−} B1-8^{hi} cells in the DZ also showed increased forward scatter, a surrogate measure of cell size (Fig. 3, O and P). Since cell size increases before the initiation of inertial cycles (Ersching et al., 2017; Finkin et al., 2019), this finding suggests that the inability of *Ccnd3*^{−/−} B cells to undergo inertial cycling results in their failure to lose cellular mass by division. We conclude that cyclin D3 is cell-intrinsically required for GC B cells to enter S phase specifically in the DZ while being dispensable for S phase entry immediately downstream of
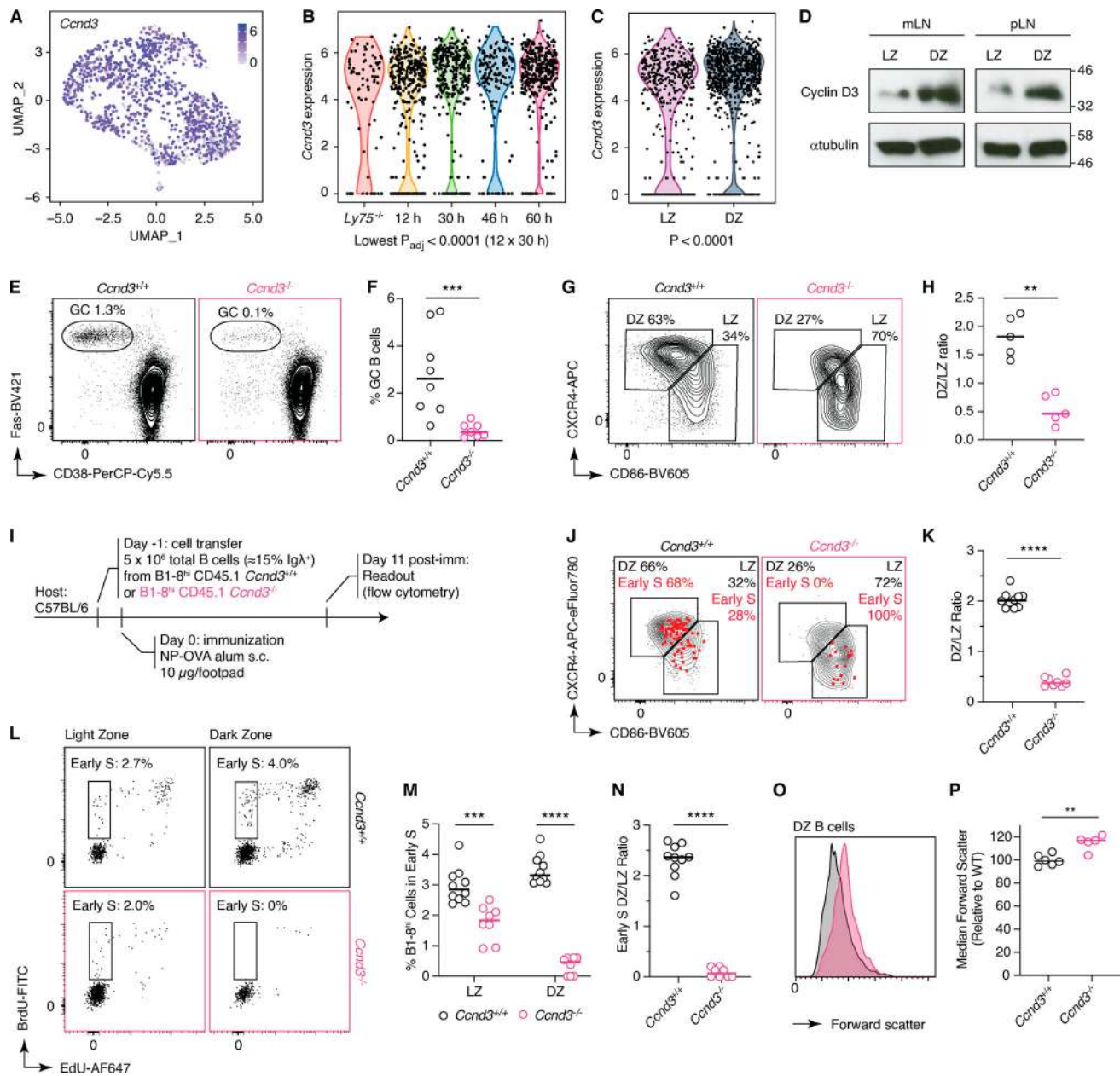
Figure 3. **Inertial B cell cycling requires cyclin D3. (A–C)** Expression of *Ccnd3* in UMAP dimension (A), over time after DEC-OVA immunization (B), and in LZ or DZ (C). P values in B are from a Kruskal–Wallis test with Dunn's multiple comparisons test. Other significant P values are <0.001 (12 × 60 h), 0.013 (*Ly75−/−* vs. 30 h), and 0.015 (*Ly75−/−* vs. 60 h). **(D)** Immunoblots of whole-cell lysates of LZ or DZ cells sorted from popliteal or mesenteric LNs (pLN or mLN, respectively). Molecular weight is indicated in kilodaltons. **(E–H)** Staining for GC (E) and DZ/LZ (G) in WT (*Ccnd3+/+*) or cyclin D3 mutant (*Ccnd3−/−*) mice that were immunized s.c. in the hind footpad for pLNs, quantified in F. **(I)** Experimental setup for induction of GCs containing WT (*Ccnd3+/+*) or cyclin D3 mutant (*Ccnd3−/−*) B1-8hi cells. **(J–P)** DZ and LZ staining of all GC B cells (black) or cells entering S phase (red; J), S phase entry (L), forward scatter (O) of WT (*Ccnd3+/+*), or cyclin D3 mutant (*Ccnd3−/−*) B1-8hi cells, quantified in K, M, N, and P. **, P < 0.01; ***, P < 0.001; ****, P < 0.0001; nonparametric Mann–Whitney test. Bars indicate median. Each circle represents a cell (B and C) or a mouse (all other figures). Data are pooled from three (E–H) or two (I–P) independent experiments. P$_{adj}$, adjusted P value; post-imm, post-immunization.

T cell–mediated selection in the LZ. This pattern implicates cyclin D3 as a nonredundant mediator of inertial cell cycles.

Cyclin D3–mediated DZ inertial cycling links GC positive selection with clonal expansion

To determine the relative importance of LZ cycles vs. inertial DZ cycles for clonal expansion, we asked whether cell proliferation

defects seen in *Ccnd3−/−* DZ B cells could be rescued by forcing strong interaction with Tfh cells using DEC-OVA (Fig. 4 A). Whereas *Ccnd3+/+* *Ly75+/+* B1-8hi cells proliferated sufficiently to outnumber *Ly75−/−* cells by fivefold over a 60-h period, clonal expansion was much less efficient when *Ly75+/+* B1-8hi cells lacked cyclin D3. With the exception of one outlier mouse, the ratio of *Ly75+/+* to *Ly75−/−* cells increased only slightly, if at all,
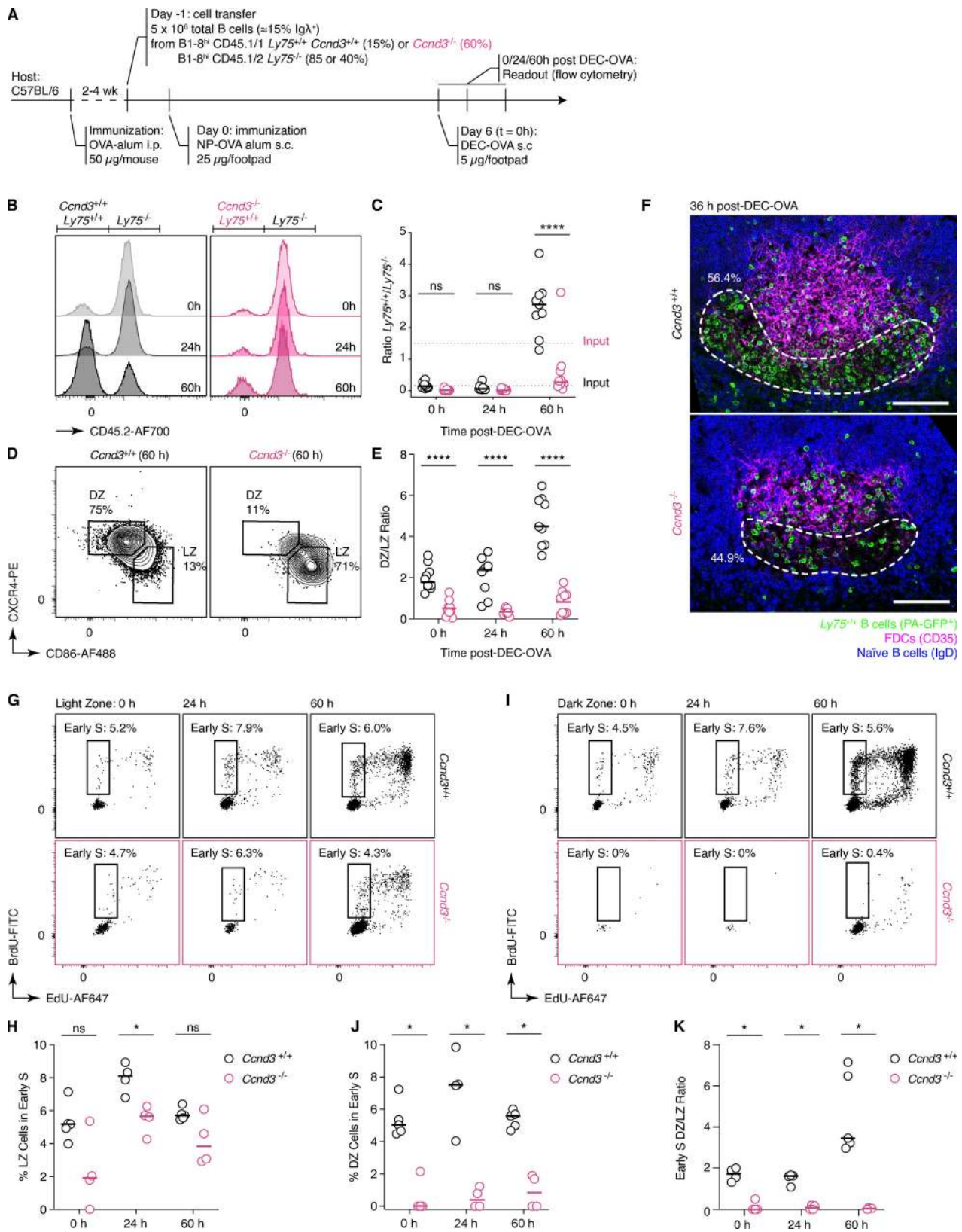
Figure 4. **Increased Tfh cell help cannot compensate for loss of cyclin D3. (A)** Experimental setup for DEC-OVA–induced positive selection of *Ly75*^{+/+} cells that are either WT (*Ccnd3*^{+/+}) or cyclin D3 mutant (*Ccnd3*^{−/−}). Note that due to of lack of competitiveness in early GC stages, *Ccnd3*^{−/−} B1-8^{hi} cells have to be transferred at a higher proportion than *Ccnd3*^{+/+} B1-8^{hi} cells. **(B–E)** Clonal expansion (B) and DZ/LZ staining (D) of WT (*Ccnd3*^{+/+}) or cyclin D3 mutant (*Ccnd3*^{−/−}) *Ly75*^{+/+} cells over time after DEC-OVA immunization, quantified in C and E. **(F)** Immunofluorescence showing the migration of WT (*Ccnd3*^{+/+}) or cyclin D3 mutant (*Ccnd3*^{−/−}) *Ly75*^{+/+} cells 36 h after DEC-OVA immunization in pLN GCs. Dotted area indicates the DZ marked by the absence of IgD (Naïve B cell marker)

over input levels (Fig. 4, B and C). Failure of $Ccnd3^{-/-}$ B cells to clonally expand was also accompanied by failure to accumulate in the DZ (Fig. 4, D and E), although histology showed that $Ccnd3^{-/-}$ cells were able to at least access the DZ anatomically at 36 h after DEC-OVA (Fig. 4 F). Even so, the proportion of early S phase cells among the $Ccnd3^{-/-}$ population dropped precipitously upon transition from the LZ to DZ, as expected given the inability of cyclin D3–deficient B cells to sustain proliferation by inertia (Fig. 4, G–K). Thus, the residual expansion of $Ccnd3^{-/-}$ $Ly75^{+/+}$ B1-8^{hi} seen in some mice can be attributed primarily to cell cycling taking place in the LZ in response to continued signals delivered by Tfh cells. We conclude that strong signaling from Tfh cells in response to DEC-OVA cannot overcome the requirement for cyclin D3 in driving DZ proliferation and that in the absence of inertial cycling, LZ cell cycles triggered directly in reaction to Tfh cell–derived signals are not sufficient to sustain large proliferative bursts.

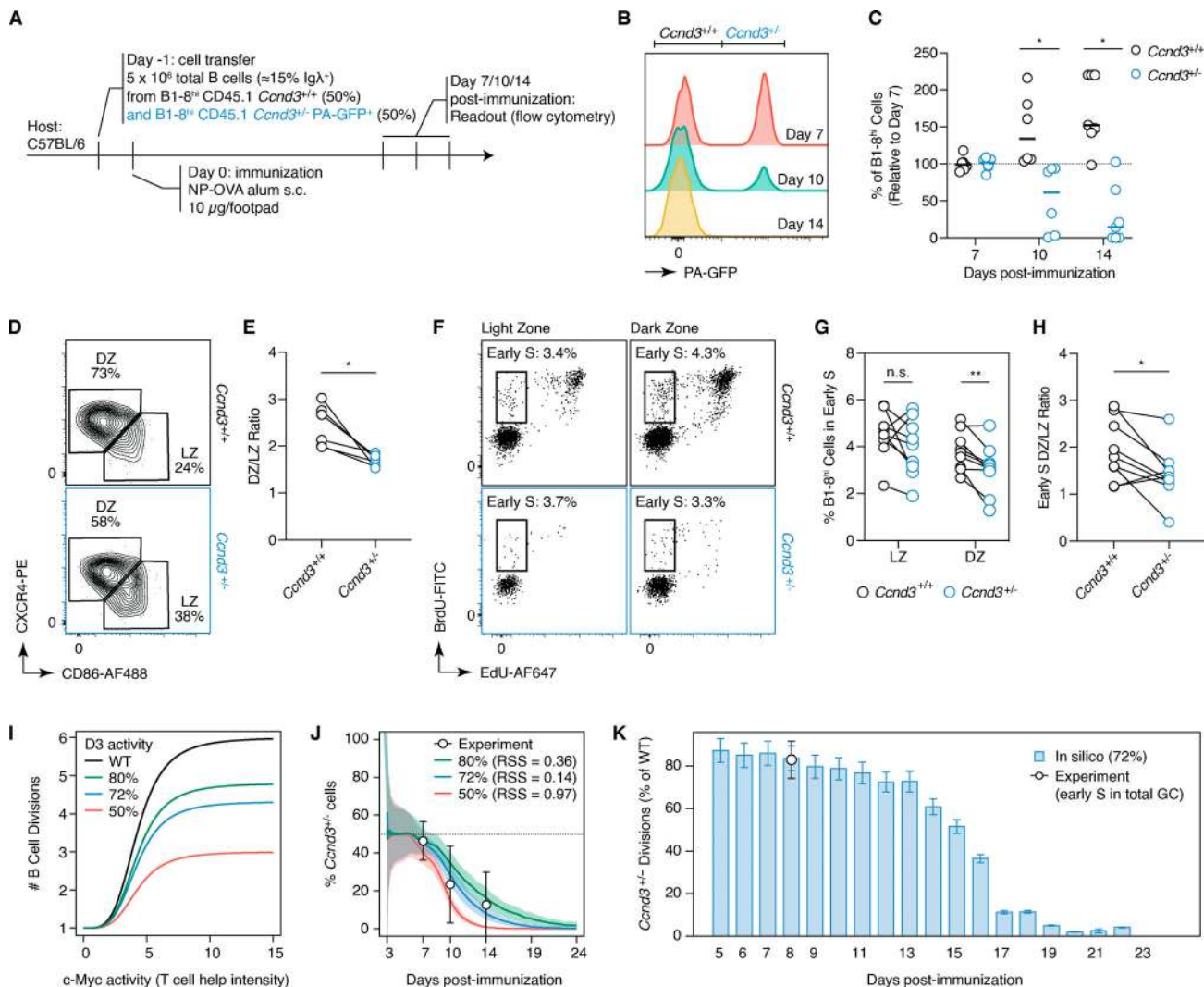### Cyclin D3 controls DZ inertial cycling in a dose-dependent manner

A potential mechanism for how the strength of the initial T cell–B cell interactions in the LZ determines the number of rounds of division that selected B cells undergo in the DZ (Gitlin et al., 2014) is that DZ B cells translate the memory of their interactions with Tfh cells into protein amounts of a cell cycle regulator. If cyclin D3 follows such a pattern, then it could be predicted that GC B cells with a higher capacity to produce cyclin D3 protein would be at a competitive advantage due to increased proliferation in the DZ. To test this, we directly competed B1-8^{hi} B cells carrying either one or two intact alleles of $Ccnd3$ by adoptive transfer of a 1:1 mixture of $Ccnd3^{+/-}$ and $Ccnd3^{+/+}$ B1-8^{hi} B cells into the same recipient mice, which were then immunized with NP-OVA in alum and assayed for relative abundance of these two populations (Fig. 5 A). Whereas both $Ccnd3^{+/+}$ and $Ccnd3^{+/-}$ B1-8^{hi} cells were found at a similar ratio in early GCs at day 7 after immunization, the proportion of $Ccnd3^{+/-}$ B1-8^{hi} cells decreased gradually over time, such that these cells were completely eliminated in three out of seven mice by day 14 after immunization (Fig. 5, B and C). Thus, the reduction in cyclin D3 dosage associated with heterozygosis is sufficient to impose a gradual but clear loss of this population from the GC. Lack of competitiveness of heterozygous B cells was associated with a slight reduction in the DZ/LZ ratio, which was already observable at day 7 after immunization (Fig. 5, D and E), and a decrease in the proportion of cells entering S phase in the DZ, but not in the LZ (Fig. 5, F–H). To extrapolate the loss of inertial proliferative capacity among $Ccnd3^{+/-}$ GC B cells from our direct competition data, we simulated this experiment in silico using a previously published agent-based model of GC selection that includes T cell control over the number of cell cycles carried a B cell undergoes upon positive selection (Meyer-Hermann, 2020

Preprint; Meyer-Hermann et al., 2012). We modeled loss of $Ccnd3$ expression as a reduction in the maximum number of divisions a $Ccnd3^{+/-}$ GC B cell can complete upon positive selection. We varied the relationship between the degree of T cell help (modeled as intensity of c-Myc activation) and the number of divisions as illustrated by the curves shown in Fig. 5 I. The experimentally measured kinetics of $Ccnd3^{+/-}$ GC B cells were best reproduced when the maximum number of divisions for $Ccnd3^{+/-}$ GC B cells in silico was reduced to 72% of WT, with a residual sum of squares (RSS) of 0.14 (Fig. 5 J). In silico, a reduction in responsiveness of this magnitude in $Ccnd3^{+/-}$ GC B cells was accompanied by a reduction in the number of cell cycles per cell to ∼84% of WT levels at day 8 after immunization, which is compatible with our EdU/BrdU incorporation data (Fig. 5 K). We conclude that cyclin D3 dose-dependently controls the number of inertial cycles a B cell will undergo in the DZ. The sensitivity of GC B cells to loss of even a single allele of $Ccnd3$ suggests that cyclin D3 protein abundance may serve as a molecular bridge linking the cumulative signal a B cell receives from T cells in the LZ and the number of cycles this cell can execute in the DZ.

A lymphoma-associated mutation that stabilizes cyclin D3 promotes DZ inertial cycling and drives clonal B cell lymphoproliferation

A parallel line of evidence pointing to the importance of cyclin D3 in GC proliferation is the presence of a series of $Ccnd3$ mutations that stabilize cyclin D3 protein in roughly 40% of cases of sporadic Burkitt lymphoma (Casanovas et al., 2004; Schmitz et al., 2012, 2014; Sonoki et al., 2001). Because Burkitt lymphoma cells closely resemble DZ B cells in gene expression (Caron et al., 2009; Victora and Mouquet, 2018), we hypothesized that stabilization of cyclin D3 by means of a lymphoma-associated mutation may increase the propensity of GC B cells to undergo inertial cycles in the DZ. To test this, we used CRISPR-Cas9–mediated genome editing to generate a $Ccnd3$ allele encoding a version of cyclin D3 protein that is stabilized by the replacement of a phosphorylatable threonine (T283A) in its C-terminal domain (Fig. 6 A). This mutation prevents phosphorylation of T283, which would otherwise promote nuclear export and proteasomal degradation of cyclin D3 (Casanovas et al., 2004; Cato et al., 2011). When introduced into the genome, the T283A mutation alone did not cause any overt anomaly in B cell development, with the possible exception of a slight increase in the percentage of pre/pro-B cells in the bone marrow (BM), nor did it lead to spontaneous GC formation in the spleens of young adult mice (Fig. S4, A and D). Nonetheless, we found that upon immunization with NP-OVA, $Ccnd3^{T283A/+}$ mice generated GCs that were approximately twice as large as WT GCs and had a markedly higher DZ/LZ ratio, suggesting increased DZ proliferation (Fig. 6, B–E). Accordingly, flow

Figure 5. **Cyclin D3 controls inertial cell cycling in a dose-dependent manner. (A)** Experimental setup for induction of GCs containing mixtures of B1-8^{hi} cells with a full ($Ccnd3^{+/+}$) or reduced ($Ccnd3^{+/-}$) dose of cyclin D3. **(B and C)** Clonal expansion of B1-8hi cells with a full ($Ccnd3^{+/+}$) or reduced ($Ccnd3^{+/-}$) dose of cyclin D3 over time, quantified in C relative to day 7. **(D and E)** DZ and LZ staining in GC B1-8hi cells 7 d after NP-OVA immunization, quantified in E. Dotted line indicates averaged DZ/LZ ratio of total GC B cells. **(F–H)** S phase entry of B1-8^{hi} cells with a full ($Ccnd3^{+/+}$) or reduced ($Ccnd3^{+/-}$) dose of cyclin D3 in LZ or DZ 8 d after NP-OVA immunization, quantified in G and H. **(I)** Relationship between strength of T cell help (modeled as c-Myc signal intensity) and number of B cell divisions in the different models used to estimate loss of function in $Ccnd3^{+/-}$ GC B cells. The maximum number of divisions allowed to $Ccnd3^{+/-}$ cells corresponds to 50% (red) or 72% (blue), or 80% (green) of the maximum number of divisions of the WT. **(J)** $Ccnd3^{+/-}$ kinetics in silico. Loss of $Ccnd3^{+/-}$ cells as a fraction of the GC population over time in silico. The maximum number of divisions of $Ccnd3^{+/-}$ GC B cells was fixed to 50% (red line), 72% (blue line), or 80% (green line) of the WT value. Mean (solid lines) and SD (shaded area) over 60 GC simulations. Experimental mean ± SD is shown as white circles. **(K)** $Ccnd3^{+/-}$ divisions in silico. The mean number of divisions of $Ccnd3^{+/-}$ cells is shown as a percentage of WT at the indicated days. Reported data result from simulations with the maximum number of divisions of the $Ccnd3^{+/-}$ GC B cells fixed to 72% of the WT maximum number of divisions. Mean and SD over 60 GC simulations. White circle represents experimental data. *, P < 0.05; **, P < 0.01; n.s., not significant, paired t test. Bars indicate median (C). Each circle represents a mouse. Data are pooled from at two independent experiments.

cytometric measurement of EdU/BrdU incorporation showed a ~50% increase in GC B cells entering S phase in the DZ but no increase in S phase entry in the LZ (Fig. 6, F–H). To confirm that the proliferative effect of cyclin D3 on the GC is B cell intrinsic, we generated mixed chimeras in which BM cells from either WT or $Ccnd3^{T283A/+}$ mice were mixed with those from B cell–deficient J_HT mice at a 20:80 ratio. Consistent with the analysis of $Ccnd3^{T283A/+}$ mice, chimeras with $Ccnd3^{T283A/+}$ B cells showed increased GC size, DZ expansion, and S phase entry in the DZ, but not in the LZ, upon immunization with NP-OVA in alum

(Fig. 6, C, E, G, and H). This phenotype was recapitulated upon immunization with KLH, ruling out any potential effects on of the hypomorphic immunoglobulin λ light chain of the SJL strain in which $Ccnd3^{T283A}$ mice were originally generated on the normally Igλ-dominated response to NP-OVA (Fig. S4, E–G). Moreover, $Ccnd3^{T283A/+}$ DZ B cells showed a decrease in size as measured by forward scatter, mirroring the phenotype found in $Ccnd3^{-/-}$ B cells (Fig. 6, I and J). This indicates that the increased proliferation of $Ccnd3^{T283A/+}$ B cells in the DZ extends to the extreme of what these cells are metabolically programmed
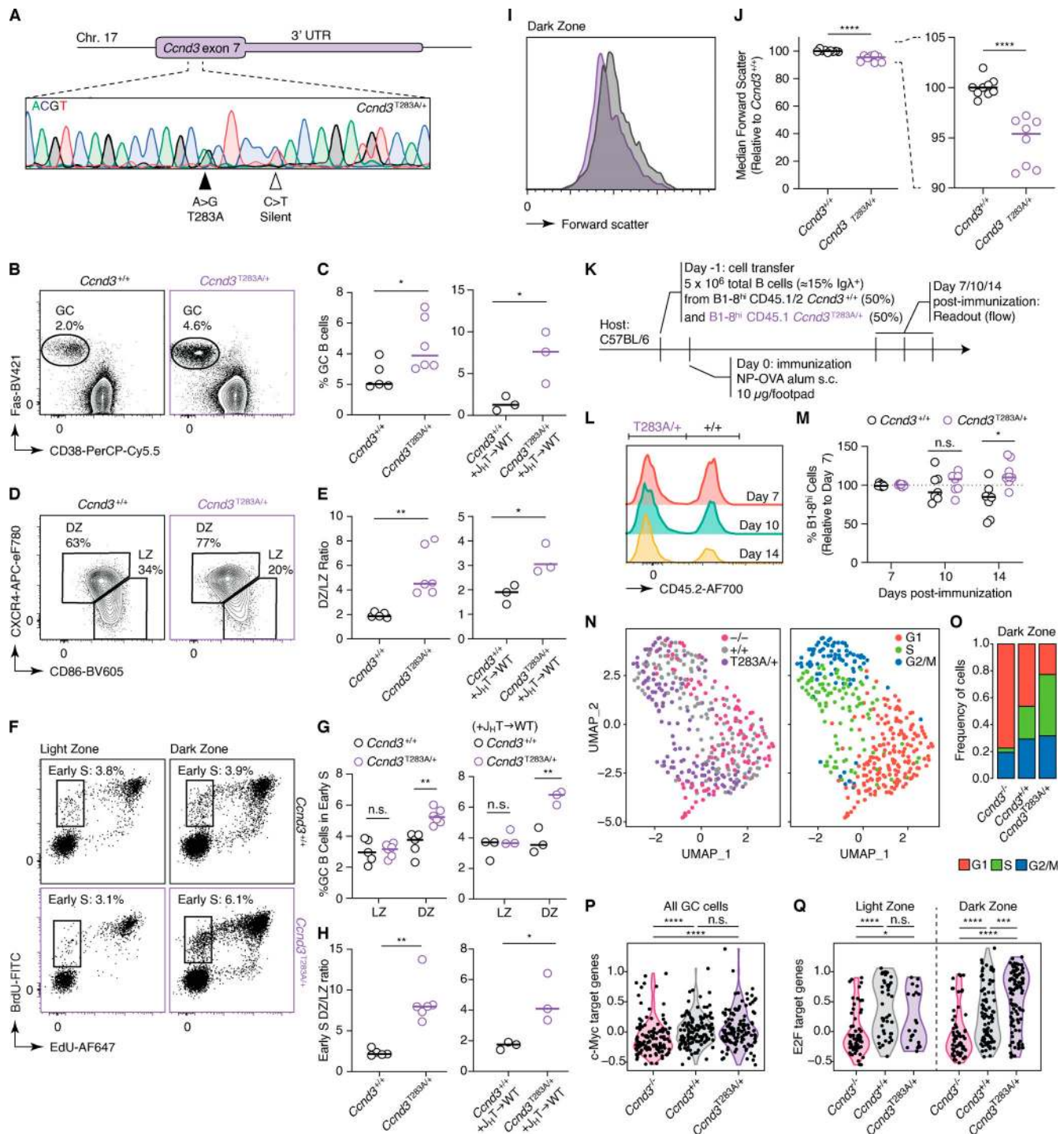
Figure 6. **A lymphoma-derived mutation in *Ccnd3* exclusively promotes inertial cell cycle entry. (A)** CRISPR/Cas9-mediated gene targeting strategy to introduce a single-nucleotide substitution resulting in a T283 to A mutation and a silent mutation to remove the protospacer adjacent motif (PAM) sequence to prevent Cas9 recutting. **(B–H)** Staining for GC (B), DZ/LZ (D), and S phase entry (F) of GC B cells in pLNs from WT (*Ccnd3*^{+/+}) or *Ccnd3*[T283A/+] mice, with quantification in C, E, G, and H. WT (*Ccnd3*^{+/+}) or *Ccnd3*[T283A/+] mice (left) or chimeras generated with BM cells isolated from WT (*Ccnd3*^{+/+}) or *Ccnd3*[T283A/+] and B cell-deficient J$_H$T mice (right) at a 20:80 ratio. **(I and J)** Forward scatter of DZ B cells sorted from pLNs of WT (*Ccnd3*^{+/+}) or *Ccnd3*[T283A/+] mice (I), with quantification of median forward scatter of DZ B cells in J. **(K)** Experimental setup for induction of GCs containing mixtures of B1-8^{hi} cells with a full (*Ccnd3*^{+/+}) or increased (*Ccnd3*[T283A/+]) dose of cyclin D3. **(L and M)** Clonal expansion of B1-8^{hi} cells with a full (*Ccnd3*^{+/+}) or increased (*Ccnd3*[T283A/+]) dose of cyclin D3 over time (L), quantified in M relative to day 7. **(N)** UMAP plot colored by genotype (left) or cell cycle phase (right). **(O)** Distribution of cell cycle phase in each genotype. **(P and Q)** Quantification of c-Myc (P) or E2F (Q) target gene signatures in in each genotype. *, P < 0.05; **, P < 0.01; ***, P < 0.001; ****, P < 0.0001; n.s., nonsignificant, nonparametric Mann–Whitney test (C, E, G, H, J, P, and Q), or paired *t* test comparison between WT (*Ccnd3*^{+/+}) or *Ccnd3*[T283A/+] cells in the same animal (M). Bars indicate median. Each circle represents a cell (P and Q) or a mouse (all other figures). Data pooled from two (B–H), three (I and J), two (L–M), or one (N–Q) independent experiments.

to support (Ersching et al., 2017). Accordingly, adoptive transfer of a 1:1 mixture of $Ccnd3^{+/+}$ and $Ccnd3^{T283A/+}$ B1-8^{hi} B cells into the same recipient mice followed by immunization with NP-OVA in alum showed that the representation of $Ccnd3^{T283A/+}$ B1-8^{hi} cells in GCs increased gradually but only slightly over time, suggesting that the proliferative capacity endowed by the $Ccnd3^{T283A}$ mutation remains limited by metabolic capacity (Fig. 6, K–M). Together, these data indicate that T283A mutation in cyclin D3 specifically promotes inertial DZ cell cycle progression in a B cell–intrinsic manner, leading to increased competitiveness of mutant B cells in the GC.

To understand the effect of cyclin D3 dosage on GC B cell cycles at the transcriptional level, we performed scRNA-seq on individually sorted $Ccnd3^{+/+}$, $Ccnd3^{-/-}$, and $Ccnd3^{T283A/+}$ GC B cells. Whereas these cells segregated primarily by cell cycle phase rather than genotype (Fig. 6 N), we found that an increase in cyclin D3 dosage resulted in a marked shift in the fraction of DZ B cells from G1 to S and G2/M phases (Fig. 6 O), suggesting that DZ B cells with high expression of cyclin D3 are poised to undergo inertial cycling and swiftly transit between S and M phases with only a brief or indiscernible G1 phase. Consistent with the inertial cell cycling phenotype revealed by DEC-OVA treatment, E2F target gene expression levels in single cells increased in a cyclin D3 dose-dependent manner in the DZ, despite comparable expression of c-Myc target genes across all genotypes (Fig. 6, P and Q). We conclude that whereas c-Myc can behave as a "charger" that prompts primary cycling in the LZ, sustained E2F target gene expression downstream of cyclin D3 dosage provides the mechanism enabling inertial cycling in the DZ.

The finding that a common lymphoma mutation (Schmitz et al., 2012) increases the ability of GC B cells to undergo inertial cell cycles suggests that lymphomas may specifically coopt the mitogen-independent proliferative program that characterizes the GC DZ to achieve sustained and rapid proliferation. To determine the long-term effects of the $Ccnd3^{T283A}$ mutation on B cell proliferation and lymphomagenesis, we aged cohorts of $Ccnd3^{T283A/+}$ mice for up to ~1.5 yr. The T283A mutation in cyclin D3 was not sufficient to cause overt morbidity or early mortality (Fig. 7 A). However, we found that B cells from $Ccnd3^{T283A/+}$ mice, but not their WT littermate controls, developed a population of Fas^{+} CD38^{+} double-positive (DP) B cells whose frequency increased over time (Fig. 7, B and C). Sequencing of the Igh genes of DP B cells revealed that this population became largely monoclonal as its size increased (Fig. 7, D and E; and Data S2), implicating $Ccnd3^{T283A}$ as a driver of B cell lymphoproliferation and also suggesting that additional mutations are likely required to achieve this phenotype. In the two mice with the largest DP population, expanded clones were class switched, heavily mutated, and present within populations with a more typical GC phenotype (Fas^{+} CD38^{-}), indicative of GC origin (Fig. 7, D and F). In the most extreme case, DP and GC B cells isolated from various tissue sources together comprised a phylogenetic tree that was both heavily expanded and highly branched, indicating continual proliferation and SHM (Fig. 7 F). In addition to the clonal DP lymphoproliferative phenotype, aged $Ccnd3^{T283A}$ mice displayed other key signs of hematopoietic

malignancy that were not observed in any of their WT counterparts. These included expansion of abnormal lymphocyte populations, enlarged secondary lymphoid organs with disrupted morphology, and lymphocytic infiltration into non-lymphoid organs, such as the liver, lungs, and kidneys (Fig. S5). While the variable nature of the malignant phenotypes observed precluded us from carrying out a systematic characterization of these outgrowths, these data confirm the oncogenic potential of $Ccnd3^{T283A}$ in lymphoid cells. We conclude that the hyper-activation of cyclin D3 by the T283A mutation promotes the acquisition of a clonal lymphoproliferative phenotype by B cells and more generally favors malignant transformation of lymphocyte populations.

Discussion

A central question in GC biology is how antigen-dependent signals delivered to GC B cells lead to the rapid clonal expansion that characterizes positive selection of higher-affinity SHM variants. Within the framework of Tfh cell–driven B cell selection, this question can be translated into how Tfh cell help delivered in the LZ controls the number of cell cycles a B cell subsequently undergoes after transition to the DZ (Mesin et al., 2016). Because this number is proportional to the push a B cell receives from Tfh cells while in the LZ (Gitlin et al., 2014, 2015; Meyer-Hermann et al., 2012; Victora et al., 2010) and our antibody blocking experiments formally rule out that DZ-initiated cell cycles depend on continued presence of Tfh cell help, we refer to DZ cell cycles as inertial. According to such a model, GC B cells would alternate between primary cell cycles in which a single S phase entry occurs in the LZ in direct response to mitogenic signals delivered at least in part by Tfh cells and inertial cycles in which B cells reenter S phase in the DZ a number of times proportional to the Tfh cell help they received in the LZ but independently of continued Tfh cell help.

Our findings show that primary (LZ) and inertial (DZ) cell cycles differ with respect to their molecular requirements. A number of studies have pointed toward c-Myc as a critical regulator of the DZ proliferative burst (Calado et al., 2012; Dominguez-Sola et al., 2012; Ersching et al., 2017; Finkin et al., 2019). Previous work suggests that c-Myc partners with mTORC1 to fuel the cellular growth that precedes the proliferative burst and dose dependently controls burst magnitude (Ersching et al., 2017; Finkin et al., 2019). However, expression of Myc c-Myc itself is not a driver of the DZ cell cycle, since its expression is predominantly found in the LZ (Calado et al., 2012; Dominguez-Sola et al., 2012; Victora et al., 2010), suggesting that inertial cycles require additional molecular drivers. Our scRNA-seq experiments show that the expression of Myc and c-Myc–dependent genes in the DZ is enriched in cells in S phase at earlier time points after positive selection, whereas inertial cycling persists for longer, likely relying on signals that are still active during G2/M (Spencer et al., 2013). Previous studies have reported stabilized expression of E2F transcription factors during mitosis in association with shortening of G1 and faster S phase entry in the subsequent cell cycle (Clijsters et al., 2019; Sigl et al., 2009). Thus, we propose that these molecular
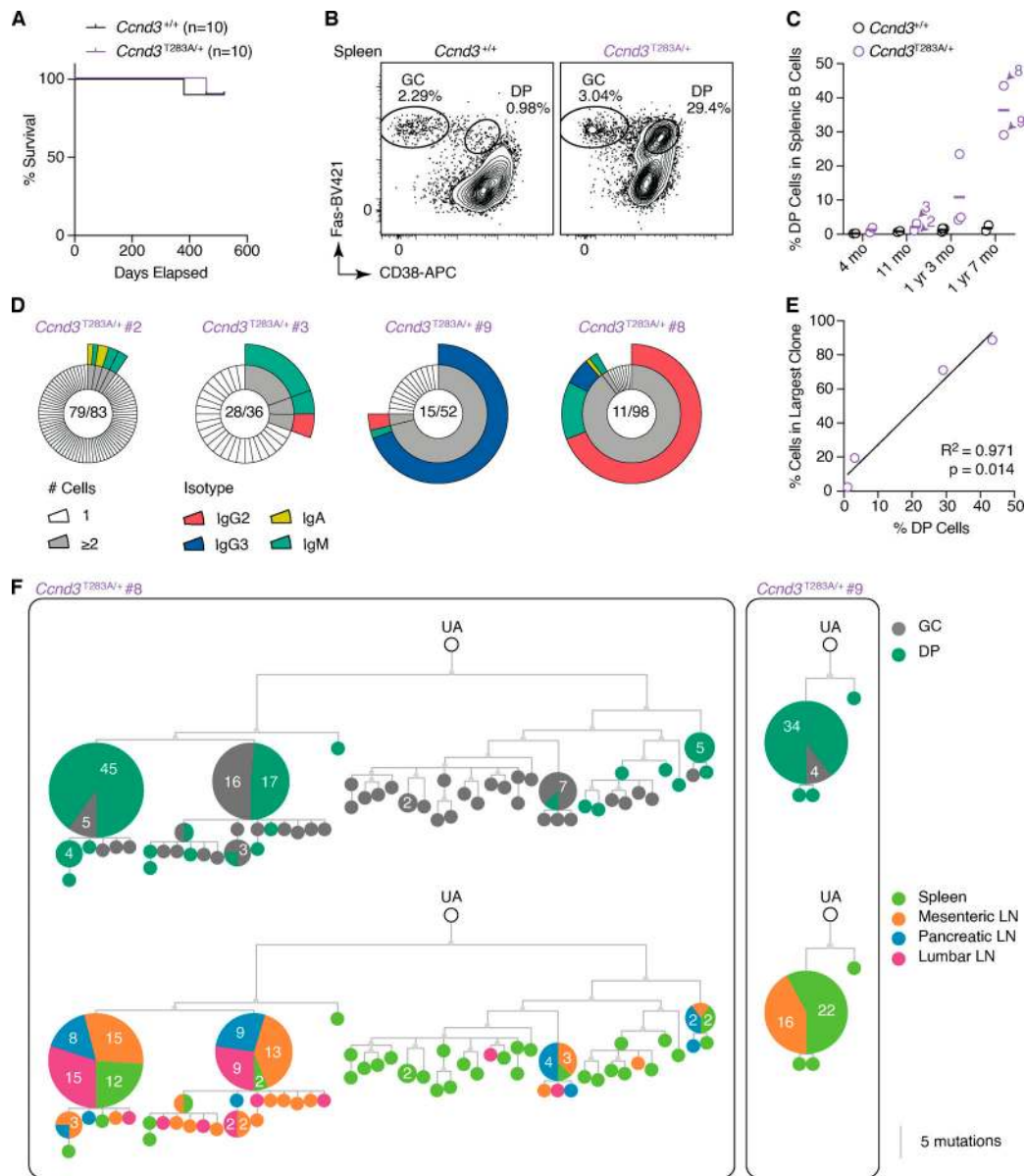
Figure 7. A lymphoma-derived mutation in *Ccnd3* drives clonal B cell lymphoproliferation. (A) Survival curve of WT (*Ccnd3*^{+/+}) or *Ccnd3*[T283A/+] mice. **(B and C)** Staining for GC/DP in splenic B cells (B), quantified in C by the age of mice. Mice indicated by arrowheads/numbers were chosen for sequencing of the *Igh* genes. **(D)** Pie chart showing clonal distribution of DP cells from spleen and mesenteric LNs. *Ccnd3*[T283A/+] #8 also includes DP cells from pancreatic and lumbar LNs. Each slice in inner rings represents one clone indicated by a distinct V(D)J rearrangement; outer rings are isotypes represented in each clone found in at least two cells. Numbers are (clones observed)/(cells sequenced). **(E)** Proportional relationship between percentage of DP cells among B220^{+} B cells and percentage of cells in the largest clone identified in each mouse. **(F)** Trees showing phylogenetic relationships between V_H sequences of cells from selected clones and their unmutated V_H ancestor (UA). Numbers inside cells indicate frequency of a particular sequence observed in combination with a GC/DP phenotype (top) or across various tissues (bottom) from the same mouse. Scale bar indicates five mutations.

signatures may characterize DZ B cells that are fated to undergo one or more subsequent rounds of cell cycling by inertia. On the other hand, DZ B with low levels of E2F would be expected to pause in G1 and migrate back to the LZ for another round of antigen-driven selection.

We find that B cell–intrinsic expression of cyclin D3 is specifically required for inertial DZ cycles, whereas it plays at best a partly redundant role in the cell cycles initiated in the LZ. Our experiments with a series of *Ccnd3* alleles with varying degrees of mRNA and protein expression show that cyclin D3 controls

the extent of DZ B cell proliferation and the size of the GC DZ in a dose-dependent manner, with fully deficient cells being almost completely unable to initiate S phase in the DZ and heterozygous B cells showing ~70% of the proliferative ability of WT cells. This suggests an instructive role for cyclin D3 in controlling GC B cell burst size. A possible mechanism for this control is that the intensity of a B cell's interaction with Tfh cells is converted to a proportionate amount of cyclin D3 protein by increased translation of mostly unchanging levels of *Ccnd3* mRNA or by stabilization of cyclin D3 protein by preventing its degradation by the

ubiquitin-proteasome system, potentially with an additional contribution of increased transcription of the *Ccnd3* gene. Previous work has shown that cyclin D1 levels carry through mitosis to accelerate subsequent S phase entry (Min et al., 2020). Our data suggest that a similar mechanism, driven by cyclin D3, may be at play in DZ inertial cycles.

A clear indication of the importance of cyclin D3 to GC B cell proliferation, especially in the DZ, is the frequent presence of *Ccnd3*[T283A] or functionally equivalent mutations in Burkitt lymphoma (Schmitz et al., 2012, 2014), the most DZ-like of B cell malignancies (Caron et al., 2009; Victora et al., 2012). The strong selection for this mutation in Burkitt lymphoma suggests that these cells may take advantage of the GC inertial cycling program to amplify the number of divisions they can undergo in response to the *Myc-Igh* translocation that defines this malignancy. Whereas mice bearing the *Ccnd3*[T283A] mutation did not succumb to B cell lymphoma, they did develop large age-related expansions of B cell clones that spanned the typical GC (FAS^{+} CD38^{−}) and an unusual FAS^{+} CD38^{+} DP phenotype, with isotype and somatic mutation patterns suggestive of GC origin. Similar DP B cells comprised four out of nine CD19^{+} lymphomas arising in mice with p53-deficient B cells upon *Plasmodium falciparum* infection (Robbiani et al., 2015). The finding that most cells in mice with large DP expansions derived from a single clone suggests that increased inertial proliferation downstream of the cyclin D3 T283A mutation may predispose B cells to acquire further somatic mutations or chromosomal rearrangements that lead to the lymphoproliferative phenotype, and may also more rapid proliferation downstream of the acquisition of secondary mutations. The oncogenic potential of this mutation is underscored by the development of various forms of hematopoietic abnormalities in *Ccnd3*[T283A] mice. Understanding the molecular drivers of inertial vs. signal-dependent cell cycling and how and why these are coopted by lymphoid malignancies may shed light on vulnerabilities that are specific to inertially cycling cells, providing an avenue that could be exploited therapeutically.

Finally, from the perspective of GC selection, the failure of *Ccnd3*^{−/−} GC B cells to clonally expand even upon strong induction of selective signals by DEC-OVA suggests that inertial cell cycles are required for the "clonal busting" that leads to optimal expansion of higher-affinity B cell clones in physiological settings (Tas et al., 2016). GC B cells appear to balance clonal bursting with other, less exclusive forms of selection as a strategy to evolve high-affinity clones while maintaining some degree of clonal diversity (Amitai et al., 2017; Bannard and Cyster, 2017; Mesin et al., 2016; Tas et al., 2016). Control of inertial selection by cyclin D3 may play an important role in fine-tuning this balance.

Materials and methods
Mice
C57BL6/J and B6.SJL mice were purchased from Jackson Labs (strain numbers 000664, 002014, and 022486, respectively). PA-GFP (Victora et al., 2010), B1-8[hi] (Shih et al., 2002), *Ly75*^{−/−} (Inaba et al., 1995), and *Ccnd3*^{−/−} (Kozar et al., 2004) mice were bred and maintained in our laboratory. Some of the B1-8[hi] *Ly75*^{−/−} mice used in scRNA-seq analysis also carried a FUCCI-

Green (fluorescent ubiquitination-based cell cycle indicator) allele (Sakaue-Sawano et al., 2008), which was not used in the analysis (see Table S1). *Ccnd3*[T283A] mice were generated in C57BL6 × SJL F1 zygotes and backcrossed onto a C57BL6 background throughout the duration of the study, and all experiments shown use backcross generations N1 to N8. Backcross generations used in this study is as follows: N8 for B1-8[hi] cell transfer (Fig. 6, K–M), N4 to N6 for early S phase entry (Fig. 6, B–G), N6 for scRNA-seq analysis (Fig. 6, N–Q), N1 for the longitudinal survival curve (Fig. 7 A), and N1 or N5 for clonal expansion and tumor formation analysis (Fig. 7, B–F; and Fig. S5). Mice were *H2*[s/b] for the longitudinal survival curve and *H2*[b/b] in all other experiments. Littermate mice were used as controls in all cases. For direct competition assays (Fig. 5 A, Fig. 6 K, and Fig. S3 M), we alternately labeled WT and mutant cells using a PA-GFP transgene or CD45.1/2 congenic markers in order to avoid any technical bias that could be introduced with a given transgene. All mice were housed in groups of two to five animals per cage in specific pathogen–free facilities at The Rockefeller University. All protocols were approved by The Rockefeller University Institutional Animal Care and Use Committee. 6–8-wk-old male and female mice were used in all experiments, except for adoptive transfers, when all recipient mice were males.

Cell transfers, immunizations, and treatments
Spleens were dissected from mice of the indicated genotype, mashed, and filtered through a 40-μm cell strainer, red blood cells were lysed with ACK buffer (Lonza), and resulting cell suspensions were filtered into PBS supplemented with 0.5% BSA and 2 mM EDTA (PBE). Naive B cells were isolated by negative selection with magnetic cell separation using anti-CD43 beads (Miltenyi), according to manufacturer's manual. Prior to cell transfer, percentage of NP-binding B1-8[hi] cell were determined by staining a fraction of cells with 5 mg/ml NP(19)-PE (Biosearch Technologies) and analyzing by flow cytometry.

To induce GCs, where indicated, male C57BL/6 recipient mice were first primed i.p. with 50 mg OVA in alum (Thermo Fisher Scientific) at 2:1 vol/vol ratio in 100 μl total volume 2–4 wk before cell transfer. Isolated B1-8^{hi} B cells were adoptively transferred at the indicated proportions as depicted in experimental setup of each figure. 1 d after adoptive cell transfer, mice were immunized with 10 μg NP(19)-OVA (NP-OVA; Biosearch Technologies) absorbed in alum or 25 μg NP-OVA for primary or boosting, respectively, by a s.c. injection into the hind footpad. Where indicated, 6 d after immunization with NP-OVA, 5 μg DEC-OVA, produced in our laboratory as previously described (Pasqual et al., 2015), in PBS was injected s.c. into the hind footpad. To block CD40L (Fig. 1), mice were injected i.v. with 200 μg of a CD40L blocking antibody (Clone MR-1; BioXCell) or 200 μg Armenian hamster IgG isotype control (BioXCell) at the indicated time points. To block MHC class II (Fig. 1), mice were injected i.v. with 200 μg of an MHC class II (I-A/I-E) blocking antibody (clone M5/115; BioXCell) or 200 μg of rat IgG2b isotype control (clone LTF-2; BioXCell) at the indicated time points.

Palbociclib (PD-0332991; SelleckChem) was diluted at 6 mg/ml in PBS, and 270 μl was injected i.p., for a total dose of 1.6 mg or 80 mg/kg.

Flow cytometry and cell sorting

Cell suspensions were resuspended in PBE and incubated on ice for 30 min with fluorescently labeled antibodies (Table S2) along with 1 mg/ml anti-CD16/32 (24G2; eBioscience).

For detection of cells in early S of the cell cycle, we performed dual nucleotide pulse and staining as previously described (Gitlin et al., 2014). Briefly, mice were injected i.v. with 1 mg of EdU (A10044; Thermo Fisher Scientific) and 1 h later with 2 mg BrdU (B5002; Sigma). 30 min after the second injection, LNs were harvested, and single-cell suspensions were prepared. After cell surface receptor staining as described above, cells were fixed and permeabilized using BD Cytofix/Cytoperm fixation and permeabilization solution and BD Cytoperm Permeabilization Buffer PLUS, respectively. EdU and BrdU incorporation into DNA was assayed using the Click-iT Plus EdU Alexa Fluor 647 Flow Cytometry Assay Kit (Invitrogen) and FITC BrdU Flow Kit (BD), respectively.

For single-cell sorting, cells were stained as above and index-sorted directly into 96-well plates containing Buffer TCL (Qiagen) supplemented with 1% β-mercaptoethanol using a BD FACS Aria II. Each plate contained all conditions assayed in each replicate. Cells were washed, filtered, and resuspended in PBE before analysis or sorting on BD FACS LSR II, FACS Symphony, or FACS ARIA II cytometers. All data were analyzed using FlowJo software v.10.

Library preparation for scRNA-seq

Libraries were prepared as previously described (Trombetta et al., 2014). Briefly, nucleic acids were extracted from sorted single cells using RNAClean XP Solid Phase Reversible Immobilization (SPRI) beads (Beckman Coulter), and RNA was hybridized first using RT primer (/5BiosG/AAGCAGTGGTATCAACGCAGAGTACTTTTTTTTTTTTTTTTTTTTTTTTTTTTTTTTTVN) and then reverse transcribed into cDNA using TSO primer (5′-AAGCAGTGGTATCAACGCAGAGTACATrGrGrG-3′) and RT maxima reverse transcription (Thermo Fisher Scientific). cDNA was amplified using ISPCR primer (5′-AAGCAGTGGTATCAACGCAGAGT-3′) and KAPA HiFi HotStart ReadyMix (Thermo Fisher Scientific), cleaned up using RNAClean XP SPRI beads three times, and tagmented using Nextera XT DNA Library Preparation Kit (Illumina). For each sequencing batch, up to four plates were barcoded at a time with Nextera XT Index Kit v2 Sets A–D (Illumina). Finally, dual-barcoded libraries were pooled and sequenced using Illumina Hiseq2500 (experiment 1)/Nextseq 550 (experiments 2–4) platform.

scRNA-seq analysis

Raw fastq sequence files generated from Smartseq2 libraries were aligned to mouse genome (v. mm10) with the annotated transcriptome (v. gencode M22) using STAR (v. 2.6; Dobin et al., 2013). Subsequently, genome-mapped BAM files were processed through RSEM (v. 1.3.1; Li and Dewey, 2011) for gene quantification. The matrix of gene counts was then, used as input for analysis by the R package Seurat (v. 3.1.4.; Stuart et al., 2019). Next, the dataset was corrected by using the regularized negative binomial regression (SCTransform) implemented by Seurat (Hafemeister and Satija, 2019). To control the dataset for unwanted sources of experimental variation, we fed the

mitochondrial gene abundance and the experimental batches information into SCTransform. Additionally, cells containing more than 20% of sequence reads aligned to mitochondrial genes were excluded before normalization. Next, single cells were clustered and gene expression was evaluated with the Seurat workflow. Gene signature scoring was performed by using Seurat's AddModuleScore function (see Data S1 for the complete list).

Immunoblotting

Cells were lysed in ice-cold lysis buffer containing 50 mM Hepes (pH 7.4), 40 mM NaCl, 2 mM EDTA, 1.5 mM sodium orthovanadate, 50 mM NaF, 10 mM pyrophosphate, 10 mM glycerophosphate, and 1% Triton X-100, as well as one tablet of EDTA-free complete protease inhibitors (Roche) per 25 ml. Cell lysates were cleared by centrifugation at 15,000 g for 10 min. Proteins lysates were denatured in sample buffer, boiled for 5 min, resolved by SDS-PAGE, transferred onto polyvinylidene difluoride membranes, and probed with the indicated antibodies.

Generation of Ccnd2-null and Ccnd3[T283A] mice

$Ccnd2$-null and $Ccnd3$[T283A] mice were generated by CRISPR/Cas9–mediated genome targeting at the Whitehead Institute for Biomedical Research and The Rockefeller University, respectively. For $Ccnd2$ targeting, cytoplasmic injection of Cas9 mix into fertilized C57BL6 zygotes at the one-cell stage was performed as previously described (Wang et al., 2013; Yang et al., 2013). The Cas9 mix contained Cas9 mRNA and chimeric sgRNA that was in vitro transcribed from a synthetic dsDNA template (gBlock; Integrated DNA Technologies) using the MEGAshortscript T7 Transcription Kit (Thermo Fisher Scientific) and purified using MEGAclear Transcription Clean-Up Kit (Thermo Fisher Scientific). $Ccnd3$[T283A] mice were generated in C57BL6 × SJL F1 zygotes using the Easi-CRISPR protocol (Quadros et al., 2017). Cas9 mix contained a CRISPR RNA (crRNA)/transactivating crRNA (tracrRNA) complex and a 200-bp repair oligo centered on the introduced mutations, synthesized as a PAGE-purified single-stranded DNA ultramer (all synthesized by Integrated DNA Technologies).

The dsDNA template for chimeric sgRNA transcription used for $Ccnd2$ was 5′-cgctgttaatacgactcactatagggACATCCAACCGTACATGCGCgttttagagctagaaatagcaagttaaaataaggctagtccgttatcaacttgaaaaagtggcaccgagtcggtgctttt-3′ (protospacer sequence in capital letters). The crRNA protospacer sequence used for $Ccnd3$ was 5′-GTGAATGGCTGTGACATCTG-3′. The repair oligo for $Ccnd3$[T283A] was 5′-gatcgaagctgccctcagggagagcctcagggaagctgctcagacagccccagcccagtgcccaaagcccccgggctctagTagTcaAgggcccagtcagaccagcGctccTacagatgtcacagccattcacctgtagcttgagacaggccctctcaggccaccaagcagaggaggggccc ctgccacccctccc-3′ (differences from original C57BL6 sequence are in capital letters).

Generation of mixed BM chimeras

BM cells were isolated from of punctured tibiae and femurs dissected from mice of indicated $Ccnd3$ genotype, as well as J_HT mice, by centrifugation at up to 10,000 g for 10 s followed by lysis of red blood cells using ACK buffer. BM cells isolated from $Ccnd3$ were mixed with those from J_HT mice at 20:80 ratio. Prior

to BM cell transfer, recipient mice were irradiated twice at 520 rad 4 h apart.

Histological analysis of tissue sections

For immunofluorescence, LNs were dissected and immediately fixed in PBS containing 4% paraformaldehyde and 10% sucrose for 1 h at 4°C. Fixed tissues were then incubated in 30% sucrose in PBS overnight at 4°C, embedded in optimum cutting temperature compound the following day, and sliced into 20-μm sections using a Leica Cryostat Microtome. For immunostaining, tissue sections were fixed in ice-cold acetone for 10 min at −20°C, blocked with Streptavidin/Biotin Blocking Kit (Vector Laboratories), and incubated with indicated antibodies diluted in PBS containing 5% BSA and 10% normal goat serum. Sections were mounted in Fluoromount-G (Southern Biotech) before imaging on a Zeiss 700 confocal microscope using a 20× objective with numerical aperture of 0.8. Post-acquisition analysis was performed using ImageJ (National Institutes of Health; http://rsb.info.nih.gov/ij/).

For H&E and immunohistochemical staining, organs were fixed in 4% formaldehyde and embedded in paraffin. 5-μm sections of mouse tissue was deparaffinized and heat antigen retrieved in citrate buffer, pH 6.4, and endogenous peroxidase (HRP) activity was blocked by treating the sections with 3% hydrogen peroxide in methanol. Indirect immunohistochemistry was performed using biotinylated peanut agglutinin followed by avidin–horseradish peroxidase or avidin-AP and developed by Vector Blue or DAB color substrates (Vector Laboratories). Sections were counterstained with hematoxylin. Images were acquired using a Zeiss Axioskop imaging microscope.

Single-cell Igh sequencing

Libraries were prepared as previously described (Mesin et al., 2020). Briefly, nucleic acids were extracted from sorted single B cells and reverse transcribed into cDNA using RT maxima reverse transcription (Thermo Fisher Scientific) and oligo(dT) primer. Ig heavy chains were amplified by PCR using a consensus forward primer for all V regions and reverse primers specific for each isotype. In the next round of PCR, 5-nucleotide barcodes were introduced using forward and reverse primers to identify the plate number/row position and column position, respectively. In the last round of PCR, Illumina paired-end sequencing adapters were incorporated. PCR products were then pooled, cleaned up using SPRI beads, and sequenced using a 500-cycle Reagent Nano kit v2 on the Illumina Miseq platform according to the manufacturer's instructions.

Mathematical modeling

For mathematical modeling to reproduce the percentage of the $Ccnd3^{+/-}$ GC B cells during the GC reaction described in vivo, we used a previously reported agent-based model for simulating the GC reaction with the DisseD framework (Meyer-Hermann, 2020 Preprint), with modifications. Specifically, the in silico simulation was initiated with 50% WT and 50% $Ccnd3^{+/-}$ B cells, for which the maximum number of divisions executed in response to Tfh cell help was fixed to a decreasing series of percentages

(80%, 76%, 72%, 71%, 60%, and 50%) of the maximum number allowed to the WT B cells, with the function regulating the number of divisions modified accordingly (Fig. 6 I). For each defined percentage, we performed 60 in silico simulations, and the best model was selected based on the lowest RSS (Eq. 1):

$$RSS = \sum_{i=1}^{N} \frac{(y_{i_d} - y_{i_s})^2}{\sigma_{i_d}^2}, \qquad (1)$$

where y_{i_d} and y_{i_s} are the experimental and simulated results, respectively, σ_{i_d} is the SD of the experimental data, and N is the sample size ($n = 3$).

Statistical analysis

Pairs of samples were compared using the Mann–Whitney U nonparametric test. Multiple comparisons were performed using the Kruskal–Wallis nonparametric test with Dunn's multiple comparison test. P values are reported as nonsignificant when P ≥ 0.05. All statistical analyses were performed using GraphPad Prism v. 8 software or RStudio. Graphs were plotted using Prism v. 8, RStudio, or GCtree and formatted using Adobe Illustrator CS.

Data availability

Sequence data have been deposited in the National Center for Biotechnology Information Gene Expression Omnibus database under accession no. GSE162182.

Online supplemental material

Fig. S1 shows the kinetics of the GC B cell response to DEC-OVA. Fig. S2 shows transcriptional signatures up-regulated by positively selected B cells in different clusters and at different time points. Fig. S3 shows B cell selection and S phase entry in $Ccnd2^{-/-}$ mice. Fig. S4 shows development and GC formation, and Fig. S5 shows disease phenotype, in $Ccnd3^{T283A/+}$ mice. Table S1 lists samples included in scRNA-seq analysis. Table S2 lists antibodies used in the study. Data S1 shows a list of cell cycle genes, Myc signature genes, E2F target genes, and mTOCR1 target genes used in scRNA-seq analysis. Data S2 shows Igh sequences obtained from $Ccnd3^{T283A/+}$ mice.

References

Amitai, A., L. Mesin, G.D. Victora, M. Kardar, and A.K. Chakraborty. 2017. A Population Dynamics Model for Clonal Diversity in a Germinal Center. *Front. Microbiol.* 8:1693. https://doi.org/10.3389/fmicb.2017.01693

Bannard, O., and J.G. Cyster. 2017. Germinal centers: programmed for affinity maturation and antibody diversification. *Curr. Opin. Immunol.* 45:21–30. https://doi.org/10.1016/j.coi.2016.12.004

Bannard, O., R.M. Horton, C.D. Allen, J. An, T. Nagasawa, and J.G. Cyster. 2013. Germinal center centroblasts transition to a centrocyte phenotype according to a timed program and depend on the dark zone for effective selection. *Immunity.* 39:912–924. https://doi.org/10.1016/j.immuni.2013.08.038

Calado, D.P., Y. Sasaki, S.A. Godinho, A. Pellerin, K. Köchert, B.P. Sleckman, I.M. de Alborán, M. Janz, S. Rodig, and K. Rajewsky. 2012. The cell-cycle regulator c-Myc is essential for the formation and maintenance of germinal centers. *Nat. Immunol.* 13:1092–1100. https://doi.org/10.1038/ni.2418

Caron, G., S. Le Gallou, T. Lamy, K. Tarte, and T. Fest. 2009. CXCR4 expression functionally discriminates centroblasts versus centrocytes within human germinal center B cells. *J. Immunol.* 182:7595–7602. https://doi.org/10.4049/jimmunol.0804272

Casanovas, O., M. Jaumot, A.B. Paules, N. Agell, and O. Bachs. 2004. P38SAPK2 phosphorylates cyclin D3 at Thr-283 and targets it for proteasomal degradation. *Oncogene.* 23:7537–7544. https://doi.org/10.1038/sj.onc.1208040

Cato, M.H., S.K. Chintalapati, I.W. Yau, S.A. Omori, and R.C. Rickert. 2011. Cyclin D3 is selectively required for proliferative expansion of germinal center B cells. *Mol. Cell. Biol.* 31:127–137. https://doi.org/10.1128/MCB.00650-10

Clijsters, L., C. Hoencamp, J.J.A. Calis, A. Marzio, S.M. Handgraaf, M.C. Cuitino, B.R. Rosenberg, G. Leone, and M. Pagano. 2019. Cyclin F Controls Cell-Cycle Transcriptional Outputs by Directing the Degradation of the Three Activator E2Fs. *Mol. Cell.* 74:1264–1277.e7. https://doi.org/10.1016/j.molcel.2019.04.010

Cyster, J.G., and C.D.C. Allen. 2019. B Cell Responses: Cell Interaction Dynamics and Decisions. *Cell.* 177:524–540. https://doi.org/10.1016/j.cell.2019.03.016

De Silva, N.S., and U. Klein. 2015. Dynamics of B cells in germinal centres. *Nat. Rev. Immunol.* 15:137–148. https://doi.org/10.1038/nri3804

Dobin, A., C.A. Davis, F. Schlesinger, J. Drenkow, C. Zaleski, S. Jha, P. Batut, M. Chaisson, and T.R. Gingeras. 2013. STAR: ultrafast universal RNA-seq aligner. *Bioinformatics.* 29:15–21. https://doi.org/10.1093/bioinformatics/bts635

Dominguez-Sola, D., G.D. Victora, C.Y. Ying, R.T. Phan, M. Saito, M.C. Nussenzweig, and R. Dalla-Favera. 2012. The proto-oncogene MYC is required for selection in the germinal center and cyclic reentry. *Nat. Immunol.* 13:1083–1091. https://doi.org/10.1038/ni.2428

Eisen, H.N. 2014. Affinity enhancement of antibodies: how low-affinity antibodies produced early in immune responses are followed by high-affinity antibodies later and in memory B-cell responses. *Cancer Immunol. Res.* 2:381–392. https://doi.org/10.1158/2326-6066.CIR-14-0029

Ersching, J., A. Efeyan, L. Mesin, J.T. Jacobsen, G. Pasqual, B.C. Grabiner, D. Dominguez-Sola, D.M. Sabatini, and G.D. Victora. 2017. Germinal Center Selection and Affinity Maturation Require Dynamic Regulation of mTORC1 Kinase. *Immunity.* 46:1045–1058.e6. https://doi.org/10.1016/j.immuni.2017.06.005

Finkin, S., H. Hartweger, T.Y. Oliveira, E.E. Kara, and M.C. Nussenzweig. 2019. Protein Amounts of the MYC Transcription Factor Determine Germinal Center B Cell Division Capacity. *Immunity.* 51:324–336.e5. https://doi.org/10.1016/j.immuni.2019.06.013

Gitlin, A.D., Z. Shulman, and M.C. Nussenzweig. 2014. Clonal selection in the germinal centre by regulated proliferation and hypermutation. *Nature.* 509:637–640. https://doi.org/10.1038/nature13300

Gitlin, A.D., C.T. Mayer, T.Y. Oliveira, Z. Shulman, M.J. Jones, A. Koren, and M.C. Nussenzweig. 2015. HUMORAL IMMUNITY. T cell help controls the speed of the cell cycle in germinal center B cells. *Science.* 349:643–646. https://doi.org/10.1126/science.aac4919

Hafemeister, C., and R. Satija. 2019. Normalization and variance stabilization of single-cell RNA-seq data using regularized negative binomial regression. *Genome Biol.* 20:296. https://doi.org/10.1186/s13059-019-1874-1

Inaba, K., W.J. Swiggard, M. Inaba, J. Meltzer, A. Mirza, T. Sasagawa, M.C. Nussenzweig, and R.M. Steinman. 1995. Tissue distribution of the DEC-205 protein that is detected by the monoclonal antibody NLDC-145. I. Expression on dendritic cells and other subsets of mouse leukocytes. *Cell. Immunol.* 163:148–156. https://doi.org/10.1006/cimm.1995.1109

Kozar, K., M.A. Ciemerych, V.I. Rebel, H. Shigematsu, A. Zagozdzon, E. Sicinska, Y. Geng, Q. Yu, S. Bhattacharya, R.T. Bronson, et al. 2004. Mouse development and cell proliferation in the absence of D-cyclins. *Cell.* 118:477–491. https://doi.org/10.1016/j.cell.2004.07.025

Li, B., and C.N. Dewey. 2011. RSEM: accurate transcript quantification from RNA-Seq data with or without a reference genome. *BMC Bioinformatics.* 12:323. https://doi.org/10.1186/1471-2105-12-323

Luo, W., F. Weisel, and M.J. Shlomchik. 2018. B Cell Receptor and CD40 Signaling Are Rewired for Synergistic Induction of the c-Myc Transcription Factor in Germinal Center B Cells. *Immunity.* 48:313–326.e5. https://doi.org/10.1016/j.immuni.2018.01.008

MacLennan, I.C. 1994. Germinal centers. *Annu. Rev. Immunol.* 12:117–139. https://doi.org/10.1146/annurev.iy.12.040194.001001

Mesin, L., J. Ersching, and G.D. Victora. 2016. Germinal Center B Cell Dynamics. *Immunity.* 45:471–482. https://doi.org/10.1016/j.immuni.2016.09.001

Mesin, L., A. Schiepers, J. Ersching, A. Barbulescu, C.B. Cavazzoni, A. Angelini, T. Okada, T. Kurosaki, and G.D. Victora. 2020. Restricted

Clonality and Limited Germinal Center Reentry Characterize Memory B Cell Reactivation by Boosting. *Cell.* 180:92–106.e11. https://doi.org/10.1016/j.cell.2019.11.032

Meyer-Hermann, M. 2020. Germinal center B cells separate signals for selection and division like compact discs. *bioRxiv.* https://doi.org/10.1101/2020.01.29.925479 (Preprint posted January 30, 2020)

Meyer-Hermann, M., E. Mohr, N. Pelletier, Y. Zhang, G.D. Victora, and K.M. Toellner. 2012. A theory of germinal center B cell selection, division, and exit. *Cell Rep.* 2:162–174. https://doi.org/10.1016/j.celrep.2012.05.010

Min, M., Y. Rong, C. Tian, and S.L. Spencer. 2020. Temporal integration of mitogen history in mother cells controls proliferation of daughter cells. *Science.* 368:1261–1265. https://doi.org/10.1126/science.aay8241

Mootha, V.K., C.M. Lindgren, K.F. Eriksson, A. Subramanian, S. Sihag, J. Lehar, P. Puigserver, E. Carlsson, M. Ridderstråle, E. Laurila, et al. 2003. PGC-1alpha-responsive genes involved in oxidative phosphorylation are coordinately downregulated in human diabetes. *Nat. Genet.* 34:267–273. https://doi.org/10.1038/ng1180

Musgrove, E.A., C.E. Caldon, J. Barraclough, A. Stone, and R.L. Sutherland. 2011. Cyclin D as a therapeutic target in cancer. *Nat. Rev. Cancer.* 11:558–572. https://doi.org/10.1038/nrc3090

Pasqual, G., A. Angelini, and G.D. Victora. 2015. Triggering positive selection of germinal center B cells by antigen targeting to DEC-205. *Methods Mol. Biol.* 1291:125–134. https://doi.org/10.1007/978-1-4939-2498-1_10

Peled, J.U., J.J. Yu, J. Venkatesh, E. Bi, B.B. Ding, M. Krupski-Downs, R. Shaknovich, P. Sicinski, B. Diamond, M.D. Scharff, and B.H. Ye. 2010. Requirement for cyclin D3 in germinal center formation and function. *Cell Res.* 20:631–646. https://doi.org/10.1038/cr.2010.55

Peng, T., T.R. Golub, and D.M. Sabatini. 2002. The immunosuppressant rapamycin mimics a starvation-like signal distinct from amino acid and glucose deprivation. *Mol. Cell. Biol.* 22:5575–5584. https://doi.org/10.1128/MCB.22.15.5575-5584.2002

Quadros, R.M., H. Miura, D.W. Harms, H. Akatsuka, T. Sato, T. Aida, R. Redder, G.P. Richardson, Y. Inagaki, D. Sakai, et al. 2017. Easi-CRISPR: a robust method for one-step generation of mice carrying conditional and insertion alleles using long ssDNA donors and CRISPR ribonucleoproteins. *Genome Biol.* 18:92. https://doi.org/10.1186/s13059-017-1220-4

Rajewsky, K. 1996. Clonal selection and learning in the antibody system. *Nature.* 381:751–758. https://doi.org/10.1038/381751a0

Reid, S., and E.C. Snow. 1996. The regulated expression of cell cycle-related proteins as B-lymphocytes enter and progress through the G1 cell cycle stage following delivery of complete versus partial activation stimuli. *Mol. Immunol.* 33:1139–1151. https://doi.org/10.1016/S0161-5890(96)00065-X

Robbiani, D.F., S. Deroubaix, N. Feldhahn, T.Y. Oliveira, E. Callen, Q. Wang, M. Jankovic, I.T. Silva, P.C. Rommel, D. Bosque, et al. 2015. Plasmodium Infection Promotes Genomic Instability and AID-Dependent B Cell Lymphoma. *Cell.* 162:727–737. https://doi.org/10.1016/j.cell.2015.07.019

Sakaue-Sawano, A., H. Kurokawa, T. Morimura, A. Hanyu, H. Hama, H. Osawa, S. Kashiwagi, K. Fukami, T. Miyata, H. Miyoshi, et al. 2008. Visualizing spatiotemporal dynamics of multicellular cell-cycle progression. *Cell.* 132:487–498. https://doi.org/10.1016/j.cell.2007.12.033

Schmitz, R., R.M. Young, M. Ceribelli, S. Jhavar, W. Xiao, M. Zhang, G. Wright, A.L. Shaffer, D.J. Hodson, E. Buras, et al. 2012. Burkitt lymphoma pathogenesis and therapeutic targets from structural and functional genomics. *Nature.* 490:116–120. https://doi.org/10.1038/nature11378

Schmitz, R., M. Ceribelli, S. Pittaluga, G. Wright, and L.M. Staudt. 2014. Oncogenic mechanisms in Burkitt lymphoma. *Cold Spring Harb. Perspect. Med.* 4:a014282. https://doi.org/10.1101/cshperspect.a014282

Schuhmacher, M., F. Kohlhuber, M. Hölzel, C. Kaiser, H. Burtscher, M. Jarsch, G.W. Bornkamm, G. Laux, A. Polack, U.H. Weidle, and D. Eick. 2001. The transcriptional program of a human B cell line in response to Myc. *Nucleic Acids Res.* 29:397–406. https://doi.org/10.1093/nar/29.2.397

Shih, T.A., E. Meffre, M. Roederer, and M.C. Nussenzweig. 2002. Role of BCR affinity in T cell dependent antibody responses in vivo. *Nat. Immunol.* 3:570–575. https://doi.org/10.1038/ni803

Shlomchik, M.J., W. Luo, and F. Weisel. 2019. Linking signaling and selection in the germinal center. *Immunol. Rev.* 288:49–63. https://doi.org/10.1111/imr.12744

Shulman, Z., A.D. Gitlin, J.S. Weinstein, B. Lainez, E. Esplugues, R.A. Flavell, J.E. Craft, and M.C. Nussenzweig. 2014. Dynamic signaling by T follicular helper cells during germinal center B cell selection. *Science.* 345:1058–1062. https://doi.org/10.1126/science.1257861

Sicinski, P., J.L. Donaher, Y. Geng, S.B. Parker, H. Gardner, M.Y. Park, R.L. Robker, J.S. Richards, L.K. McGinnis, J.D. Biggers, et al. 1996. Cyclin D2 is an FSH-responsive gene involved in gonadal cell proliferation and oncogenesis. *Nature.* 384:470–474. https://doi.org/10.1038/384470a0

Sigl, R., C. Wandke, V. Rauch, J. Kirk, T. Hunt, and S. Geley. 2009. Loss of the mammalian APC/C activator FZR1 shortens G1 and lengthens S phase but has little effect on exit from mitosis. *J. Cell Sci.* 122:4208–4217. https://doi.org/10.1242/jcs.054197

Solvason, N., W.W. Wu, N. Kabra, X. Wu, E. Lees, and M.C. Howard. 1996. Induction of cell cycle regulatory proteins in anti-immunoglobulin-stimulated mature B lymphocytes. *J. Exp. Med.* 184:407–417. https://doi.org/10.1084/jem.184.2.407

Solvason, N., W.W. Wu, D. Parry, D. Mahony, E.W. Lam, J. Glassford, G.G. Klaus, P. Sicinski, R. Weinberg, Y.J. Liu, et al. 2000. Cyclin D2 is essential for BCR-mediated proliferation and CD5 B cell development. *Int. Immunol.* 12:631–638. https://doi.org/10.1093/intimm/12.5.631

Sonoki, T., L. Harder, D.E. Horsman, L. Karran, I. Taniguchi, T.G. Willis, S. Gesk, D. Steinemann, E. Zucca, B. Schlegelberger, et al. 2001. Cyclin D3 is a target gene of t(6;14)(p21.1;q32.3) of mature B-cell malignancies. *Blood.* 98:2837–2844. https://doi.org/10.1182/blood.V98.9.2837

Spencer, S.L., S.D. Cappell, F.C. Tsai, K.W. Overton, C.L. Wang, and T. Meyer. 2013. The proliferation-quiescence decision is controlled by a bifurcation in CDK2 activity at mitotic exit. *Cell.* 155:369–383. https://doi.org/10.1016/j.cell.2013.08.062

Stuart, T., A. Butler, P. Hoffman, C. Hafemeister, E. Papalexi, W.M. Mauck III, Y. Hao, M. Stoeckius, P. Smibert, and R. Satija. 2019. Comprehensive Integration of Single-Cell Data. *Cell.* 177:1888–1902.e21. https://doi.org/10.1016/j.cell.2019.05.031

Subramanian, A., P. Tamayo, V.K. Mootha, S. Mukherjee, B.L. Ebert, M.A. Gillette, A. Paulovich, S.L. Pomeroy, T.R. Golub, E.S. Lander, and J.P. Mesirov. 2005. Gene set enrichment analysis: a knowledge-based approach for interpreting genome-wide expression profiles. *Proc. Natl. Acad. Sci. USA.* 102:15545–15550. https://doi.org/10.1073/pnas.0506580102

Tas, J.M., L. Mesin, G. Pasqual, S. Targ, J.T. Jacobsen, Y.M. Mano, C.S. Chen, J.C. Weill, C.A. Reynaud, E.P. Browne, et al. 2016. Visualizing antibody affinity maturation in germinal centers. *Science.* 351:1048–1054. https://doi.org/10.1126/science.aad3439

Tirosh, I., B. Izar, S.M. Prakadan, M.H. Wadsworth II, D. Treacy, J.J. Trombetta, A. Rotem, C. Rodman, C. Lian, G. Murphy, et al. 2016. Dissecting the multicellular ecosystem of metastatic melanoma by single-cell RNA-seq. *Science.* 352:189–196. https://doi.org/10.1126/science.aad0501

Trombetta, J.J., D. Gennert, D. Lu, R. Satija, A.K. Shalek, and A. Regev. 2014. Preparation of Single-Cell RNA-Seq Libraries for Next Generation Sequencing. *Curr. Protoc. Mol. Biol.* 107:1–17. https://doi.org/10.1002/0471142727.mb0422s107

Victora, G.D., and H. Mouquet. 2018. What Are the Primary Limitations in B-Cell Affinity Maturation, and How Much Affinity Maturation Can We Drive with Vaccination? Lessons from the Antibody Response to HIV-1. *Cold Spring Harb. Perspect. Biol.* 10:a029389. https://doi.org/10.1101/cshperspect.a029389

Victora, G.D., and M.C. Nussenzweig. 2012. Germinal centers. *Annu. Rev. Immunol.* 30:429–457. https://doi.org/10.1146/annurev-immunol-020711-075032

Victora, G.D., T.A. Schwickert, D.R. Fooksman, A.O. Kamphorst, M. Meyer-Hermann, M.L. Dustin, and M.C. Nussenzweig. 2010. Germinal center dynamics revealed by multiphoton microscopy with a photoactivatable fluorescent reporter. *Cell.* 143:592–605. https://doi.org/10.1016/j.cell.2010.10.032

Victora, G.D., D. Dominguez-Sola, A.B. Holmes, S. Deroubaix, R. Dalla-Favera, and M.C. Nussenzweig. 2012. Identification of human germinal center light and dark zone cells and their relationship to human B-cell lymphomas. *Blood.* 120:2240–2248. https://doi.org/10.1182/blood-2012-03-415380

Wang, H., H. Yang, C.S. Shivalila, M.M. Dawlaty, A.W. Cheng, F. Zhang, and R. Jaenisch. 2013. One-step generation of mice carrying mutations in multiple genes by CRISPR/Cas-mediated genome engineering. *Cell.* 153:910–918. https://doi.org/10.1016/j.cell.2013.04.025

Yang, H., H. Wang, C.S. Shivalila, A.W. Cheng, L. Shi, and R. Jaenisch. 2013. One-step generation of mice carrying reporter and conditional alleles by CRISPR/Cas-mediated genome engineering. *Cell.* 154:1370–1379. https://doi.org/10.1016/j.cell.2013.08.022
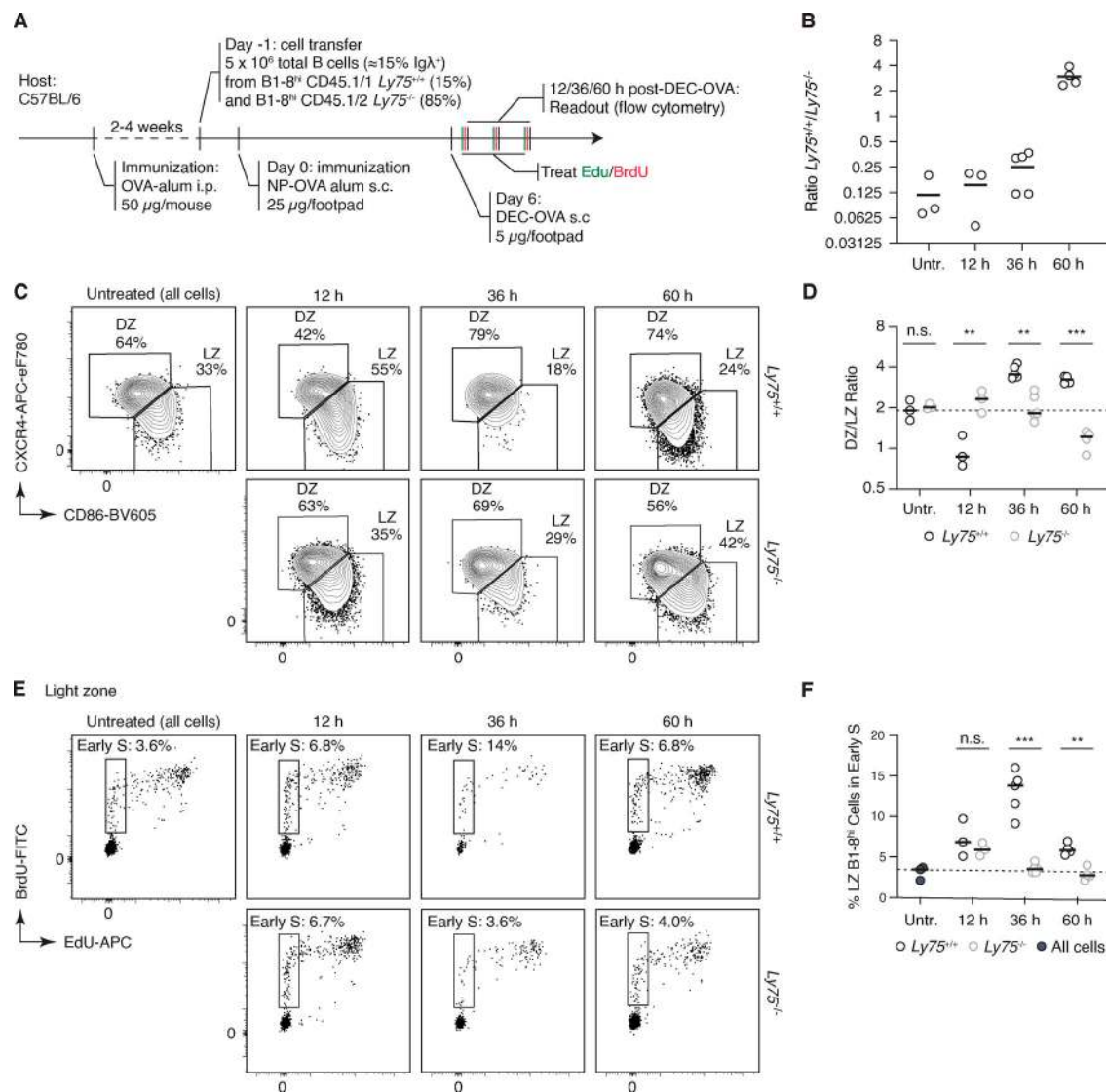
Figure S1. **Synchronization and enrichment of *Ly75*⁺/⁺ cells with DEC-OVA immunization (related to Fig. 1). (A)** Experimental setup for DEC-OVA–induced positive selection of *Ly75*⁺/⁺ GC B cells followed by double labeling with EdU/BrdU to assay for S phase entry. **(B)** Expansion of *Ly75*⁺/⁺ cells over *Ly75*⁻/⁻ over the time course. **(C and D)** DZ and LZ staining of *Ly75*⁺/⁺ and *Ly75*⁻/⁻ cells over the time course (C), quantified in D. **(E and F)** S phase entry of *Ly75*⁺/⁺ and *Ly75*⁻/⁻ B1-8hi cells in the LZ (E), quantified in F. **, P < 0.01; ***, P < 0.001; n.s., not significant; paired *t* test comparison between *Ly75*⁺/⁺ and *Ly75*⁻/⁻ cells in the same animal. Bars indicate median. Each circle represents a mouse. Data are pooled from two independent experiments. Untr., untreated.
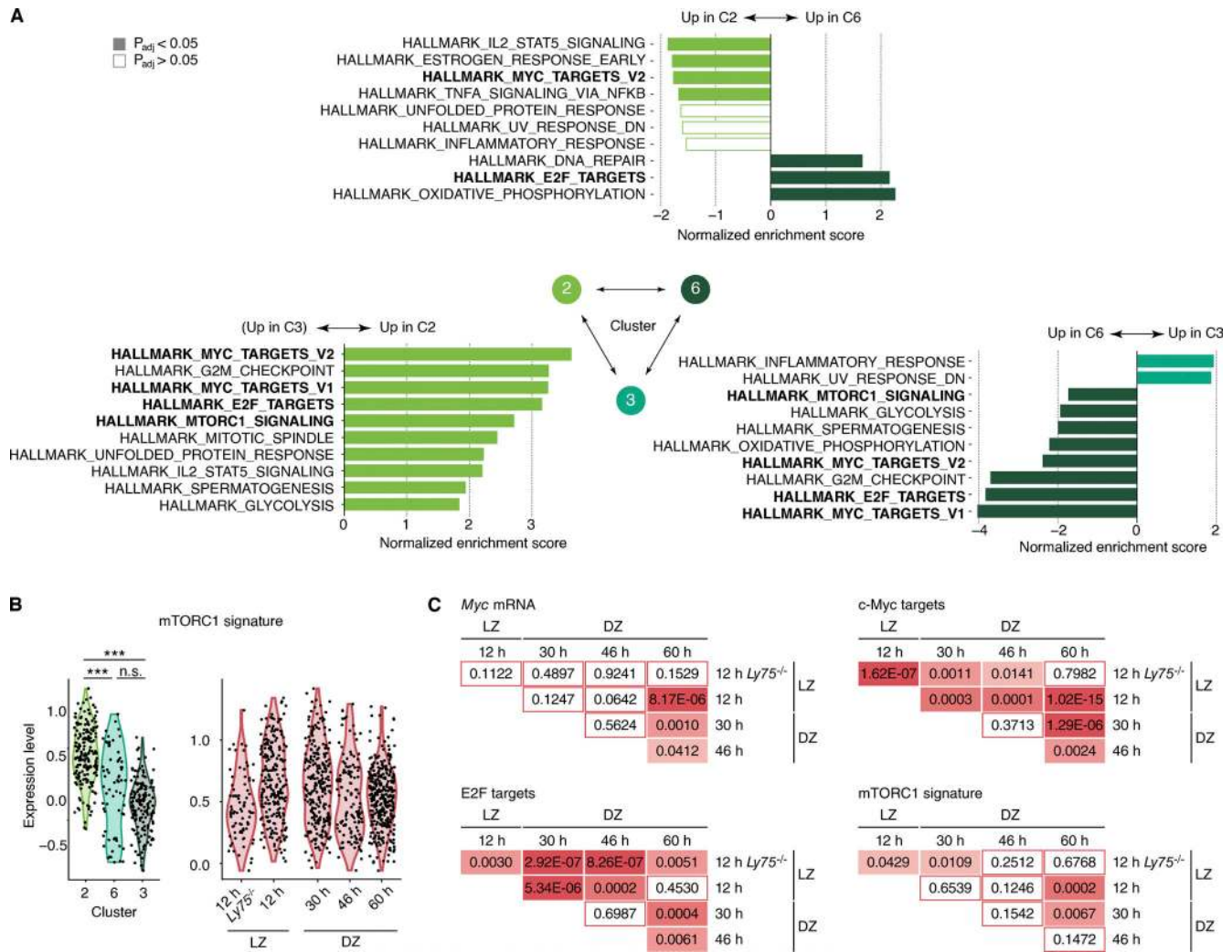
Figure S2. GSEA between the S phase clusters (related to Fig. 2). (A) Top 10 most significantly varied "hallmark" signatures from the MSigDB database using GSEA to compare clusters 2, 3, and 6 (C2, C3, and C6). Pathways that are common among three sets of comparisons are indicated in bold. **(B)** Expression of mTORC1 signature in clusters 2, 3, and 6 (left) or in DEC-OVA time points with indicated zonal phenotypes (right). **(C)** Summary of P values using Mann–Whitney U test. ***, $P < 0.001$; n.s., not significant; P_{adj}, adjusted P value.
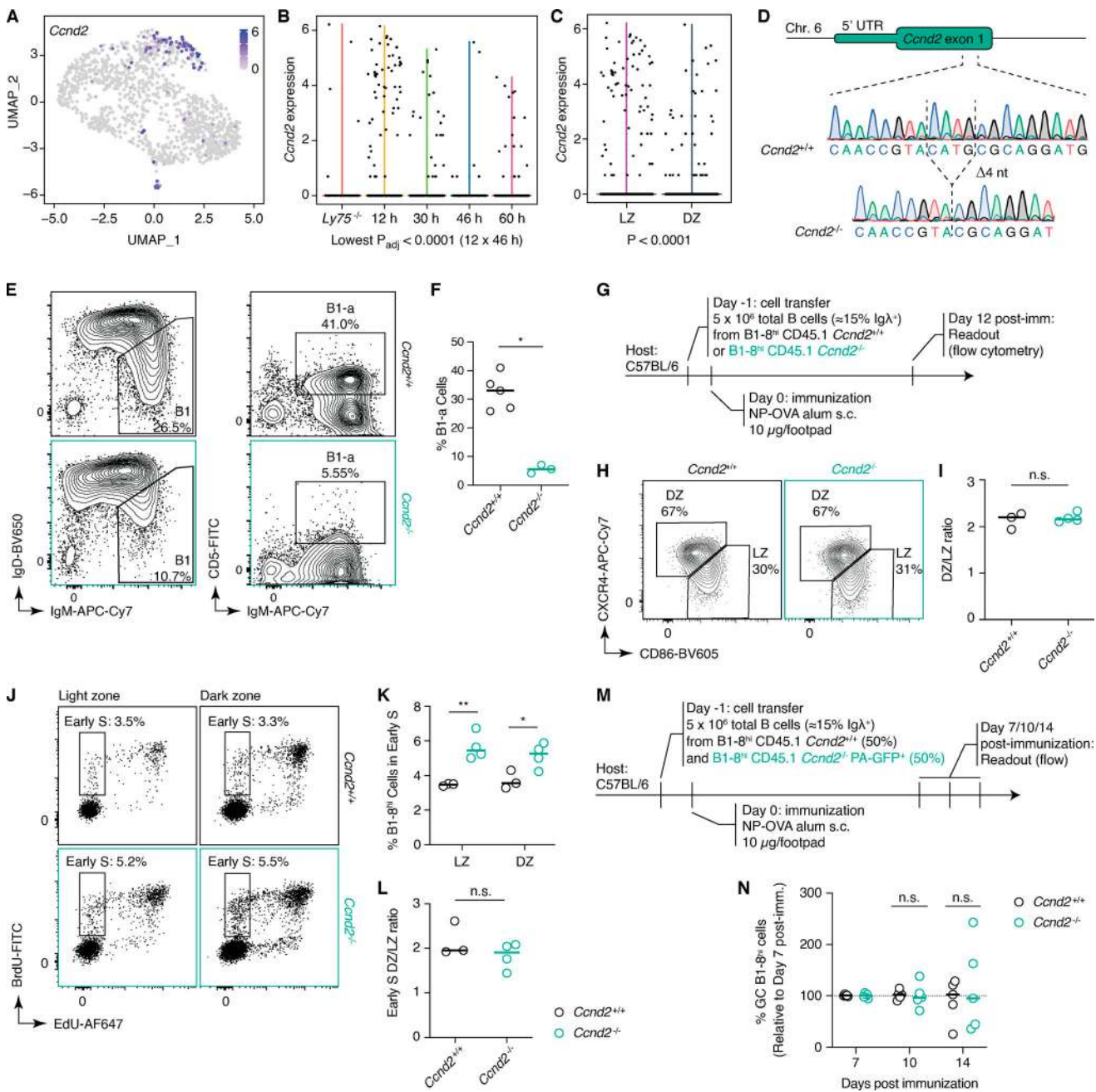
Figure S3. **Cyclin D2 is dispensable for inertial B cell cycling (related to Fig. 3). (A–C)** Expression of *Ccnd2* in UMAP dimension (A), over time after DEC-OVA immunization (B), and in LZ or DZ (C). P values in B are from a Kruskal–Wallis test with Dunn's multiple comparisons test. Other significant P values are <0.001 (12 × 60 h), 0.0013 (12 vs. 30 h), and 0.037 (*Ly75*$^{-/-}$ vs. 12 h). **(D)** CRISPR/Cas9-mediated gene targeting strategy to introduce a 4-bp deletion and premature stop codon in *Ccnd2*. **(E and F)** Staining for B1 (left) and B1-a (right) cells isolated from peritoneal cavities of WT (*Ccnd2*$^{+/+}$) or cyclin D2–deficient (*Ccnd2*$^{-/-}$; E) mice, quantified in F. **(G)** Experimental setup for induction of GCs containing WT (*Ccnd2*$^{+/+}$) or cyclin D2 mutant (*Ccnd2*$^{-/-}$) B1-8^{hi} cells. **(H–L)** DZ and LZ staining (H) and S phase entry (J) in WT (*Ccnd2*$^{+/+}$) or cyclin D2–deficient (*Ccnd2*$^{-/-}$) B1-8^{hi} GC cells 12 d after NP-OVA immunization, quantified in I, K, and L. **(M)** Experimental setup for induction of GCs containing mixtures of WT (*Ccnd2*$^{+/+}$) or cyclin D2 mutant (*Ccnd2*$^{-/-}$) B1-8^{hi} cells. **(N)** Clonal expansion of WT (*Ccnd2*$^{+/+}$) or cyclin D2 mutant (*Ccnd2*$^{-/-}$) B1-8^{hi} cells over time, relative to day 7 (represented by a dotted line). *, P < 0.05; **, P < 0.01; n.s., nonsignificant, nonparametric Mann–Whitney test, compared with WT (*Ccnd2*$^{+/+}$; G, I, and J) or day 7 (L). Bars indicate median. Each circle represents a mouse. Data are pooled from two independent experiments. P$_{adj}$, adjusted P value.
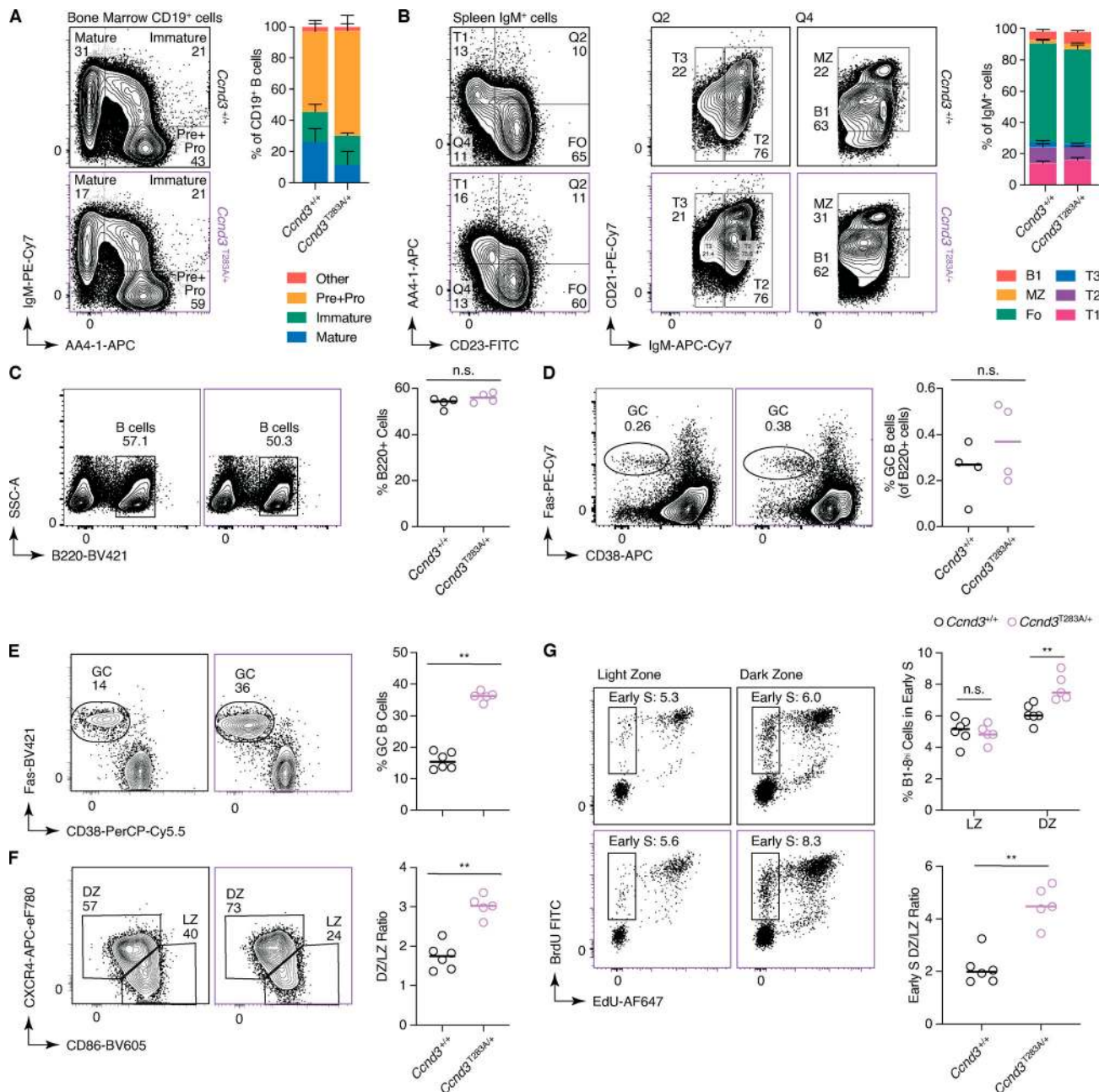
Figure S4. **Analysis of *Ccnd3*^{T283A/+} mice (related to Fig. 6). (A and B)** Bone marrow (A) and splenic (B) B cells development in distribution WT (*Ccnd3*^{+/+}) or *Ccnd3*^{T283A/+} mice (left) and quantification (right). FO, follicular; MZ, marginal zone. Bars indicate SD. **(C and D)** Staining (left) and quantification (right) of splenic B cells (C) and GC (D) in WT (*Ccnd3*^{+/+}) or *Ccnd3*^{T283A/+} mice. Bars indicate median. SSC-A, side scatter area. For A–D, 6-wk-old mice ($n = 4$ for each genotype) were sacrificed. *Ccnd3*^{T283A/+} mice used are generation N8. **(E–G)** Staining (left) and quantification (right) for GC (E), DZ/LZ (F), and S phase entry (G) of GC B cells induced upon immunization with KLH in pLNs from WT (*Ccnd3*^{+/+}) or *Ccnd3*^{T283A/+} mice. **, $P < 0.01$; n.s., nonsignificant, nonparametric Mann–Whitney test. Bars indicate median. Each circle represents a mouse. Data pooled from two independent experiments. *Ccnd3*^{T283A/+} mice used in this experiment are from generations N6 and N7.
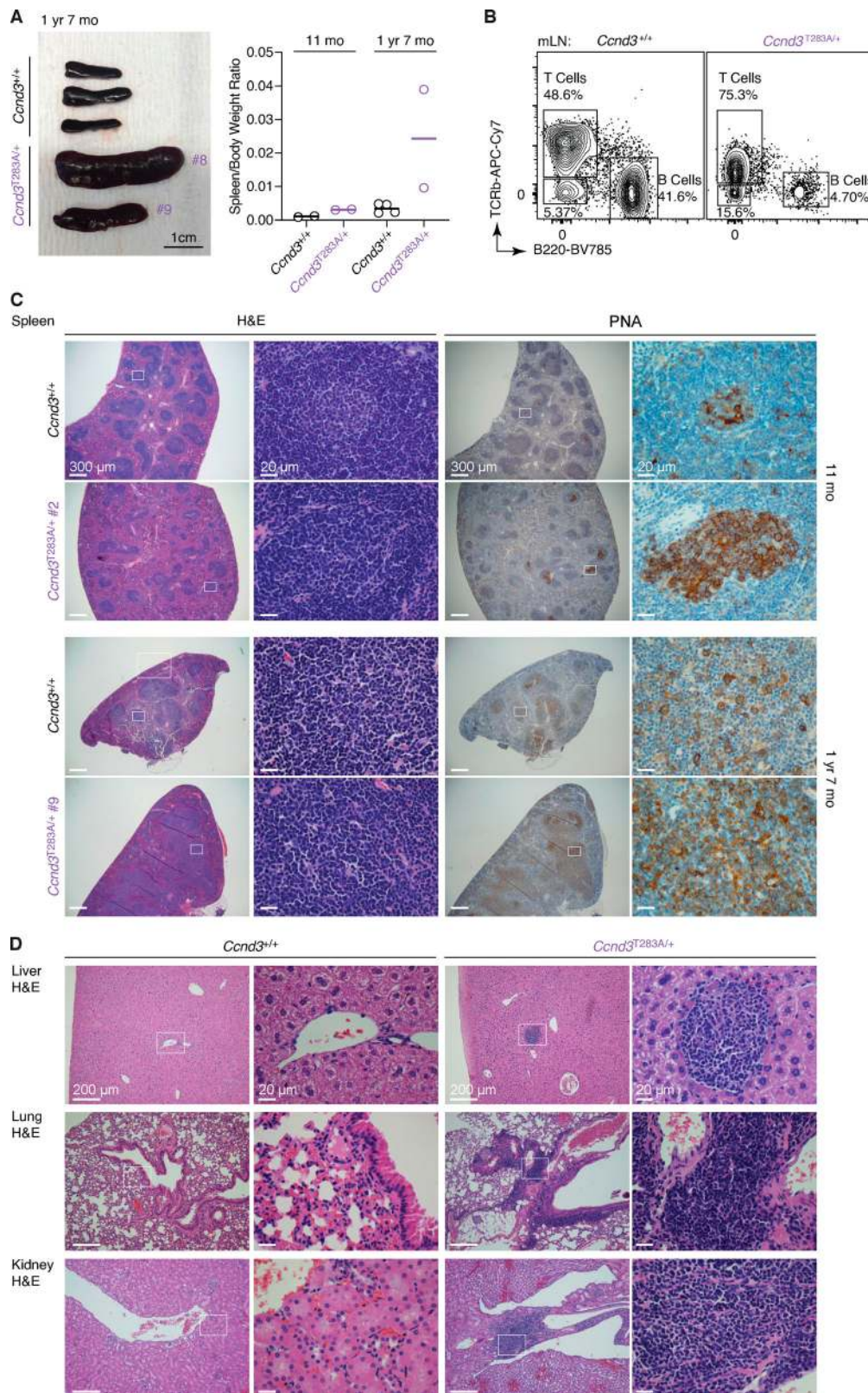
Figure S5. **Analysis of *Ccnd3*^T283A/+^ mice (related to Fig. 7). (A)** Spleens from WT (*Ccnd3*^+/+^) or *Ccnd3*^T283A/+^ animals (right) and quantification of spleen to body weight ratios (left). Bars indicate median. **(B)** B and T cell staining in WT (*Ccnd3*^+/+^) or *Ccnd3*^T283A/+^ mice revealed expansion of abnormal lymphocyte populations with diminished or no expression of TCRb/B220. **(C)** H&E and peanut agglutinin (PNA) staining of WT (*Ccnd3*^+/+^) or *Ccnd3*^T283A/+^ spleens revealed disrupted morphology. **(D)** H&E staining of nonlymphoid tissues from WT (*Ccnd3*^+/+^) or *Ccnd3*^T283A/+^ revealed lymphocytic infiltration.

Table S1 and Table S2 are provided online as separate Word files. Table S1 lists samples included in scRNA-seq analysis. Table S2 lists antibodies used in the study. Data S1 and Data S2 are provided online as separate Excel files. Data S1 shows a list of cell cycle genes, Myc signature genes, E2F target genes, and mTOCR1 target genes used in scRNA-seq analysis. Data S2 shows *Igh* sequences obtained from *Ccnd3*^{T283A/+} mice.